Available online at www.sciencedirect.com
SCIENCE DIRECT
Journal of Catalysis 241 (2006) 132–148
JOURNAL OF CATALYSIS
www.elsevier.com/locate/jcat

Absorption-enhanced reforming of phenol by steam over supported Fe catalysts

K. Polychronopoulou [a], A. Bakandritsos [b], V. Tzitzios [b], J.L.G. Fierro [c], A.M. Efstathiou [a,*]

[a] *Department of Chemistry, Heterogeneous Catalysis Laboratory, University of Cyprus, P.O. Box 20537, CY 1678 Nicosia, Cyprus*
[b] *Institute of Materials Science, NCSR Demokritos, Agia Paraskevi Attikis, GR-153 10 Athens, Greece*
[c] *Instituto de Catálisis y Petroleoquimica, CSIC, C/Marie Curie 2, Cantoblanco, 28049 Madrid, Spain*

Received 5 January 2006; revised 26 March 2006; accepted 17 April 2006

Abstract

Supported Fe catalysts of varying support chemical composition prepared by sol–gel and incipient wetness impregnation methods were studied for the steam reforming of phenol (one of the main constituents of tar produced during steam gasification of wood biomass) in the 600–700 °C range. Various natural CO_2 absorbent materials were also used together with the supported Fe catalyst in a fixed-bed microreactor to investigate the enhancement of H_2 production during short times on stream, as well as the removal of CO_2 from the reaction product gas (absorption enhanced reforming [AER]). A 5 wt% Fe/50Mg-50Ce-O catalyst was found to be the most active in terms of H_2 product yield, with one of the lowest amounts of accumulated carbonaceous deposits. Among a series of x wt% Fe/50Mg-50Ce-O ($x = 1$–10) catalysts, H_2-specific integral production rate (mol-H_2/(g s)) goes through a maximum at the 5 wt% Fe loading, whereas the largest amount of "carbon" deposits was measured on the highest Fe-loaded (10 wt%) catalyst. The stability of the 5 wt% Fe/50Mg-50Ce-O catalyst was studied during consecutive oxidation → reaction and oxidation → reduction → reaction cycles of short duration. X-Ray diffraction, X-ray photoelectron spectroscopy, and Mössbauer studies were performed for detailed physicochemical characterization of the supported Fe catalysts in their fresh and used states (after phenol steam reforming). The most active Fe-based catalyst (5 wt% Fe/50Mg-50Ce-O) was found to present a high Fe^{2+}/Fe^{3+} ratio after phenol steam reforming (Mössbauer studies). Various transient experiments demonstrated that the enhanced production of H_2 occurring in the presence of a CO_2 absorbent material (supported Fe + CO_2 absorbent) for short times on stream was due to a change in the water–gas shift reaction ($CO + H_2O \leftrightarrow CO_2 + H_2$) toward further H_2 production. The 5 wt% Fe/Mg-Ce-O catalyst was found to compete favorably with a 35 wt% Ni/γ-Al_2O_3 industrial catalyst (used for tar steam reforming) at 700 °C in terms of H_2 product yield and to have significantly lower CO/CO_2 product ratios.
© 2006 Elsevier Inc. All rights reserved.

Keywords: Phenol steam reforming; Absorption enhanced reforming (AER); Hydrogen production; Transient experiments; CO_2 absorbent; Dolomite; Olivine; Calcite

1. Introduction

Biomass is receiving increased attention as potential source of renewable energy with respect to global issues of sustainable energy [1]. Pyrolysis of biomass has several environmental advantages over fossil fuels, namely lower emissions of CO_2 and other greenhouse gases [1]. However, one of the major issues in biomass gasification is dealing efficiently with tar reduction during the process [2–4]. The product of biomass gasification contains about 5.0 wt% phenolic compounds [5,6]. Catalytic steam reforming appears to be a very attractive way to convert tar components into H_2 and other useful chemicals [7].

Despite the large number of research works concerning steam reforming of various hydrocarbons feedstock over supported-Ni [1] and precious metal catalysts [8], steam reforming over supported Fe catalysts has not yet been studied in great extent, especially for aromatic compounds. Murata et al. [9] have studied the steam reforming of iso-octane and methylcyclohexane (MCH) over Fe–Mg/γ-Al_2O_3 catalyst. The latter was active for the steam reforming of iso-octane but less ac-

* Corresponding author. Fax: +357 22 892801.
E-mail address: efstath@ucy.ac.cy (A.M. Efstathiou).

0021-9517/$ – see front matter © 2006 Elsevier Inc. All rights reserved.
doi:10.1016/j.jcat.2006.04.015

tive for the steam reforming of MCH. The steam reforming of methane has been studied over 1 wt% Fe/ZrO_2 catalyst [10] but low methane conversions were measured at 800 °C.

An alternative group of materials to supported-metals that were investigated for biomass gasification are natural materials. Calcined dolomites (MgO/CaO) and olivine are the most investigated materials, whereas various calcites are the least investigated ones [2]. Calcined dolomites have attracted much attention as catalysts in biomass gasification [11–16] due to the fact that these materials are cheap and disposable and can significantly reduce the tar content of the product gas from the gasifier. Their chemical composition depends on their origin. In general, it consists of 30 wt% CaO, 21 wt% MgO, 45 wt% CO_2, and trace amounts of minerals (e.g., SiO_2, Fe_2O_3, and Al_2O_3) [2].

Orío et al. [11] investigated four different dolomites of varying Fe_2O_3 content for oxygen/steam gasification of wood. The dolomite with the highest Fe_2O_3 content exhibited the highest activity (95% tar conversion). Aldén et al. [17] and Lammers et al. [18] investigated the catalytic reforming of naphthalene over dolomite. Conversions of 96 and 79%, respectively, were achieved using 15% CO_2 or 18% H_2O in the reaction feed stream. Simell et al. [19] investigated a Finnish dolomite with relatively high iron content (1.5 wt%) and found that reforming of toluene over dolomite at 900 °C proceeded with higher rates using CO_2 rather than steam in the feed stream, whereas dry reforming was inhibited by the presence of steam. Taralas et al. [20] used dolomite quicklime and dolomitic magnesium oxide to reform cyclohexane and *n*-heptane (model tar compounds). Delgado et al. [12] studied calcined dolomite, magnesite, and calcite for tar conversion in the 800–880 °C range in a pilot plant unit; high initial tar conversions were found, but catalyst deactivation could not be avoided.

An interesting alternative to calcined dolomite is olivine, a magnesium aluminosilicate. Rapagna et al. [21] investigated the tar-reforming activity of olivine and compared it with that of calcined dolomite. Olivine was found to be a much better attrition-resistant material in fluidized-bed reactor applications. Corella et al. [22] tested calcined dolomite, natural and sintered olivines, and Ni-olivine catalysts for biomass gasification with air and found dolomite to be 1.4 times more active than olivine.

The concept of combining reaction and separation in H_2 production technologies is not new. The first description of the conversion of hydrocarbons in the presence of steam and of CO_2 acceptor was published in 1868 [23]. Brun-Tsekhovoi et al. [24] reported significantly enhanced H_2 formation for steam reforming of CH_4 in a fluidized-bed reactor containing a Ni-based catalyst and a specially treated dolomite (CO_2 absorbent). Carvil et al. [25] described the general concept of the sorption enhanced reaction process (SERP), which uses pressure and concentration swing adsorption principles for reaction rate enhancement.

The present work is related to previous work [26–29] on the development of novel catalytic materials for the production of a hydrogen-rich gas (>90 vol% H_2) from steam gasification of wood biomass in a fast-recycled fluidized-bed reactor in a single step. To the best of our knowledge, no published works on phenol steam reforming over supported Fe catalysts coupled with the use of CO_2 absorbent natural materials exist. In the present work, various supported Fe catalysts, the supports of which were prepared by sol–gel and incipient wetness impregnation methods, were studied for steam reforming of phenol in the temperature range of 600–700 °C. Supported Rh catalysts were examined for phenol steam reforming [28,29]. These catalysts are considered ideal for fixed-bed applications to significantly reduce the tar content in the product gas stream; however, fluidized-bed applications, where catalyst mass loss is considered significant, require cheap and nontoxic catalytic materials, such as supported Fe solids.

Even though phenol was reportedly one of the major tar constituents in steam gasification of wood biomass in a fast-recycled fluidized-bed reactor [26,27], the catalytic behavior of supported Fe catalysts reported herein is likely to be affected by the presence of toluene (the second important tar compound identified [26]) and other gas products formed within the fluidized-bed reaction zone (e.g., coke formation). This important subject is under investigation.

2. Experimental

2.1. Catalysts synthesis

A 50Mg-50Ce-O mixed metal oxide (50 mol% Mg and 50 mol% Ce) was prepared by the sol–gel method using $Mg(OEt)_2$ and $Ce(NO_3)_2$ (Aldrich) as precursors of Mg and Ce, respectively. The synthesis procedure has been described elsewhere [29]. The x wt% CeO_2/γ-Al_2O_3 ($x = 10$, 20, 40) and x wt% MgO/γ-Al_2O_3 ($x = 10$, 20) supported metal oxides were prepared by the incipient wetness impregnation method using $Mg(NO_3)_2$ and $Ce(NO_3)_2$ (Aldrich) as precursors of Mg and Ce, respectively. Pure commercial γ-Al_2O_3 (Aldrich, 180 μm $< d <$ 520 μm) was used as a support after being calcined at 800 °C for 4 h. After synthesis and drying (overnight at 120 °C), all solid samples were calcined in air at 800 °C for 4 h. The samples were then slowly cooled to room temperature and stored for further use.

A series of x wt% Fe/50Mg-50Ce-O ($x = 1$, 2.5, 5.0, and 10.0) solids were prepared by the incipient wetness impregnation method using $Fe(NO_3)_3$ (Aldrich) as an iron metal precursor. A given amount of the precursor solution corresponding to the Fe loading of interest was used to impregnate the support metal oxide (in powder form) at 40 °C. After impregnation and drying overnight at 120 °C, the supported Fe catalyst was calcined in air at 600 and 800 °C for 2 h before storage and further use.

Two natural dolomites, coded as D4 and DOLII, and two calcites, coded as A2 and A3, were also studied in phenol steam reforming as catalysts themselves or as CO_2 absorbent materials in a fixed-bed catalytic microreactor that also contained a supported Fe catalyst.

2.2. Catalyst characterization

2.2.1. BET surface area, fraction of Fe metal on the surface in the fully reduced state

The specific surface areas ($m^2\,g^{-1}$) of the fresh and some of the used supported Fe catalysts were measured by N_2 adsorption at 77 K (BET method) using a multipoint Fisons Sorpty 1900 system. Before any measurements were taken, the samples were outgassed at 400 °C under vacuum ($P \approx 1.3 \times 10^{-3}$ mbar) overnight. For the x wt% CeO_2/γ-Al_2O_3 supported metal oxides, to correlate the BET area and content of ceria, the apparent specific surface area (S^{ca}_{BET}) was calculated using the following relationship [30]:

$$S^{ca}_{BET} = \frac{S_{BET}}{1 - CeO_2\,\text{content}}. \quad (1)$$

The fraction of Fe metal on the surface in the fully reduced state (Fe^0) with respect to the total Fe in the sample for the various supported Fe catalysts, after the applied H_2 reduction treatment, was determined by H_2 chemisorption according to the following procedure. The catalyst was first calcined in 20% O_2/He at 800 °C for 2 h and then reduced in 20% H_2/He at 400 °C for 4 h. After reduction, the catalyst was heated to 600 °C in He flow to desorb any H_2 that might have been spilled over the support. The catalyst was then cooled in He flow to 200 °C, and the feed was switched to a 2% H_2/He gas mixture for 30 min. The catalyst was cooled in 2% H_2/He flow to room temperature and left for 15 min. A switch to He flow was then made for 15 min; after this time, no H_2 signal could be observed with mass spectrometry. The temperature of the catalyst was then increased from room temperature to 700 °C to carry out a temperature-programmed desorption (TPD) experiment. The amount of H_2 desorbed ($\mu mol/g_{cat}$) and the Fe loading of the catalyst were used to estimate the fraction of Fe on the surface fully reduced with respect to the total Fe in the sample ($\mu mol\text{-}Fe^0_s/\mu mol\text{-}Fe$), assuming $H{:}Fe_s = 1{:}1$.

2.2.2. X-Ray diffraction analyses

The crystal structure of the fresh supported metal oxides (x wt% CeO_2/γ-Al_2O_3, y wt% MgO/γ-Al_2O_3) and that of the mixed metal oxide (50Mg-50Ce-O) prepared by the sol–gel method were checked by X-ray diffraction (XRD) with a Shimadzu 6000 diffractometer using Cu-K_α radiation (λ = 1.5418 Å). The samples were calcined in air at 800 °C for 4 h before the XRD measurements. The primary mean crystallite size (d_{XRD}) of ceria and magnesia were determined using the diffraction peaks at $2\theta = 28.55°$ and 42.9°, corresponding to the (111) CeO_2 and (200) MgO faces, respectively, and Scherrer's equation [31].

2.2.3. H_2 temperature-programmed reduction studies

H_2 temperature-programmed reduction (TPR) experiments were conducted by passing a 2 vol% H_2/He (50 NmL/min) over 0.2 g of the precalcined (20% O_2/He, 800 °C, 2 h) catalyst under a linear temperature ramp (30 °C/min). The H_2 concentration (mol%) was monitored with an on-line mass spectrometer (Omnistar, Balzers). The mass numbers (m/z) 2, 18, and 32 were used for H_2, H_2O, and O_2, respectively. Based on material balance, the rate of hydrogen consumption ($\mu mol\ H_2/(g\,min)$) versus temperature was estimated.

2.2.4. X-Ray photoelectron spectroscopy studies

X-ray photoelectron spectroscopy (XPS) studies were conducted on a VG Escalab 200 R spectrometer equipped with a hemispherical electron analyzer and an Mg-K_α (1253.6 eV) X-ray source. The XP spectrometer was equipped with a chamber for sample treatment under controlled gas atmospheres and at temperatures below 700 °C. A certain region of the XP spectrum was scanned a number of times to obtain a good signal-to-noise ratio. The binding energies (BEs) were referenced to the C 1 s peak (103.4 eV) to account for charging effects.

2.2.5. Mössbauer spectroscopy studies

Mössbauer measurements were carried out with a conventional constant acceleration spectrometer equipped with a ^{57}Co(Rh) source, calibrated with α-Fe; the isomer shifts are reported relative to these values. The spectra recorded at 298, 77, and 4 K were fitted with a least squares minimization procedure assuming Lorentzian line shapes. The fresh supported Fe catalysts investigated were reduced in H_2 at 400 °C for 2 h before any measurements, whereas no pretreatment was done for the used catalysts.

2.3. Catalytic studies

The experimental apparatus used for evaluating the catalytic performance of supported Fe and natural materials toward phenol steam reforming has been described in detail previously [28]. A 0.15-g catalyst sample in particle form (d = 0.2–0.3 mm) diluted in 0.15 g of SiO_2 was loaded into the reactor. The total gas flow rate used was 100 NmL/min (GHSV $\approx$ 80,000 h^{-1}), and the feed gas composition consisted of 0.25 vol% C_6H_5OH/20 vol% H_2O/He. The steam reforming of phenol reaction can be described by the following reaction scheme [1,2,32]:

$$C_6H_5OH + 5H_2O \rightarrow 6CO + 8H_2, \quad (2)$$

$$CO + H_2O \leftrightarrow CO_2 + H_2. \quad (3)$$

Estimation of individual conversions, X_1 and X_{WGS}, of reactions (2) and (3), respectively, based on material balances has been described previously [28,29]. The hydrogen reaction selectivity, S_{H_2}, is given by the following relationship [28]:

$$S_{H_2} = \frac{1}{2.33}\frac{F_T y_{H_2}}{6F^f_T y^f_{C_6H_5OH}}. \quad (4)$$

In Eq. (4), S_{H_2} is a selectivity parameter relative to the maximum theoretical production of hydrogen that could be obtained based on reactions (2) and (3).

Integral specific reaction rates, R_i (mol/g s) for product i (e.g., H_2), corresponding to phenol conversions >20% are estimated from material balances. Because iron (Fe^{2+}/Fe^{3+}) oxides are one of the active phases over the supported Fe catalysts investigated in the present work, where the support phases also

contribute to the catalytic activity measured, estimation of true specific reaction rates in terms of TOF (s^{-1}) is not possible.

2.4. Transient steam reforming of phenol in the presence of CO_2 absorbent

The initial transient steam reforming reaction behavior of the catalytic bed material (supported Fe + CO_2 absorbent) was studied as follows. The supported Fe catalyst was thoroughly mixed with the CO_2 absorbent material under consideration in a ratio of 1:2 (w/w), with the total amount of the catalytic bed kept constant at 0.45 g. The supported Fe catalyst and the CO_2 absorbent material used had mean particle size of 0.1 and 0.3 mm, respectively. The catalytic bed material in the absence of CO_2 absorbent consisted of 0.15 g of supported Fe and 0.3 g of SiO_2. The catalytic bed material was initially pretreated in air at 800 °C for 2 h, flushed with He for 10 min, and then cooled to 400 °C. It was then reduced in pure H_2 at 400 °C for 2 h. The reactor was then brought in He flow to the reaction temperature, and the feed was changed to the reaction gas mixture. The transient response signals of H_2, CO_2, and CO were recorded with time on stream by an on-line mass spectrometer and analyzed as described previously [28,29].

3. Results and discussion

3.1. Catalyst characterization

3.1.1. BET surface area, fraction of Fe^0 on the surface

The specific surface areas (BET) of the fresh 50Mg-50Ce-O, 10CeO_2/γ-Al_2O_3, 20CeO_2/γ-Al_2O_3, and 40CeO_2/γ-Al_2O_3 supports were found to be 79.8, 77.8, 65.2, and 44 m^2/g, respectively. The latter three BET values are not close to the BET value of γ-Al_2O_3 (100.8 m^2/g), a result that also held for the calculated specific surface area (S_{BET}^{ca}) of the ceria-loaded materials. The latter were found to be 86.4, 81.5, and 67 m^2/g for the 10CeO_2-, 20CeO_2-, and 40CeO_2-loaded γ-Al_2O_3 solids, respectively. The difference between the S_{BET} and S_{BET}^{ca} values of the ceria-loaded Al_2O_3 supports indicates that the BET area and the examined CeO_2 loadings are not proportional quantities. Closely equal values of S_{BET} of the unloaded and S_{BET}^{ca} of the corresponding metal oxide-loaded support would be expected only for high dispersions (i.e., monolayer coverage) of deposited metal oxides [30]. The ceria loading corresponding to monolayer coverage on a given γ-alumina has been reported to be approximately 6 wt% [33]. Mekhemmer et al. [34] reported the synthesis of 10 wt% CeO_2/γ-Al_2O_3 with 65 $m^2\,g^{-1}$ (calcined at 500 °C for 2 h), and Damyanova et al. [35] reported the synthesis of 12 wt% CeO_2/γ-Al_2O_3 with 143 $m^2\,g^{-1}$ (calcined at 800 °C). The S_{BET} values of the present 10MgO/γ-Al_2O_3 and 20MgO/γ-Al_2O_3 solids were found to be 76.9 and 58.2 m^2/g, respectively. The latter value is much lower than that of γ-Al_2O_3 (100.8 m^2/g), because the two oxidic phases of MgO and γ-Al_2O_3 reacted, forming a new spinel phase ($MgAl_2O_4$), as revealed by XRD studies (see Section 3.1.2). Szmigiel et al. [36] reported the synthesis of MgO/γ-Al_2O_3 with 65 m^2/g after calcination at 900 °C for 1 h.

The BET area of the fresh 5 wt% Fe/50Mg-50Ce-O catalyst was found to be 59.1 $m^2\,g^{-1}$. However, after 2 h of continuous phenol steam reforming, this BET area increased slightly, to 64.7 $m^2\,g^{-1}$, due to the presence of steam [28,29]. Calcite A2 (north Greece) and calcite A3 (central Greece) had BET areas of 6.4 and 8.1 $m^2\,g^{-1}$, respectively. The BET areas for Dolomite D4 (marble, North Greece) and dolomite DOLII (Hufgard, Germany) were 12.4 and 15.2 $m^2\,g^{-1}$, respectively. Olivine had a BET area of 0.7 $m^2\,g^{-1}$.

The fractions of Fe metal atoms on the surface fully reduced with respect to the total Fe in the sample for the fresh x wt% Fe/Mg-Ce-O solids estimated from H_2 chemisorption (see Section 2.2.1) were found to be 37.0, 31.0, 26.0, and 17.0% for the 1.0, 2.5, 5.0, and 10.0 wt% Fe-loaded catalysts, respectively.

3.1.2. XRD studies

Fig. 1 presents X-ray diffractograms of 10% CeO_2/γ-Al_2O_3 (Fig. 1b), 20% CeO_2/γ-Al_2O_3 (Fig. 1c), pure ceria (Fig. 1a), and γ-alumina (Fig. 1d). All diffraction peaks corresponding to the fluorite structure of CeO_2 (peaks 1) are visible in Figs. 1a–c. The diffraction peaks corresponding to γ-alumina (peaks 2) became more intense with decreasing CeO_2 loading. The CeO_2 crystallite size estimated from diffraction peak broadening reveals relatively smaller crystallites in the 10% CeO_2/γ-Al_2O_3 solid (10.2 nm) compared with the 20% CeO_2/γ-Al_2O_3 (12.3 nm) solid; however, sizes are notably smaller than 19.0 nm for the unsupported CeO_2 (Fig. 1a). These results agree with previous work [37], where sintering of CeO_2 crystals and surface textural changes can be avoided when ceria is loaded on a high-surface area support. However, the presence of ceria nanocrystallites with $d < 4$ nm, which escape XRD detection, cannot be excluded. Mekhemmer et al. [34] examined alumina-supported ceria prepared by the impregnation method and found a mean crystallite size of 7.5 nm after calcination at 650 °C for 2 h, a result similar to that obtained in the present work. No changes in the structural composition of the present x wt% CeO_2/γ-Al_2O_3 supports due to the presence of Fe were detected. XRD patterns obtained on 10% MgO/γ-Al_2O_3 and 20% MgO/γ-Al_2O_3 (not presented here) revealed the presence of $MgAl_2O_4$ with mean crystallite size of 6.2 and 8.0 nm, respectively. XRD of 50Mg-50Ce-O solid (sol–gel) revealed diffraction peaks corresponding to pure MgO ($d = 24.5$ nm)

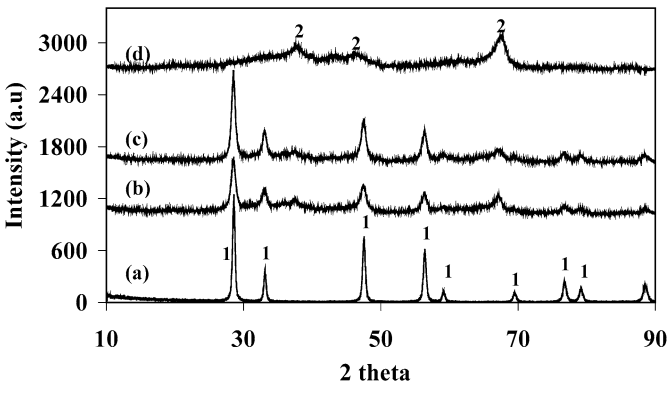

Fig. 1. X-Ray diffraction patterns of (a) CeO_2, (b) 10 wt% CeO_2/γ-Al_2O_3, (c) 20 wt% CeO_2/γ-Al_2O_3, (d) γ-Al_2O_3.

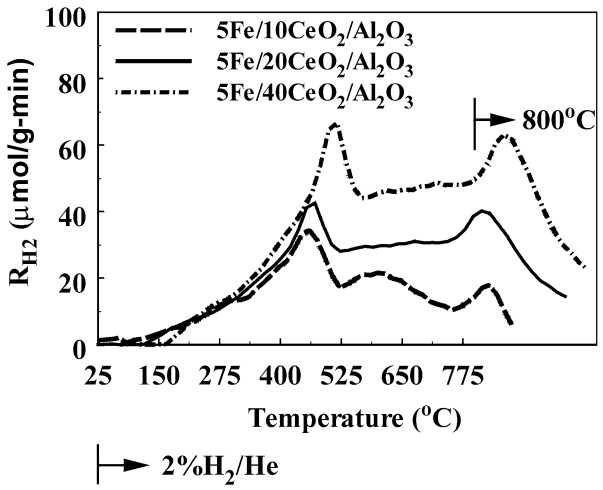

Fig. 2. Hydrogen temperature-programmed reduction (H_2-TPR) traces in terms of rate of hydrogen consumption (μmol-H_2/(g min)) versus temperature obtained on the 5 wt% Fe/x wt% CeO_2-Al_2O_3 (x = 10, 20, 40) catalysts. $F_{H_2/He} = 50$ NmL/min, $\beta = 30\,^{\circ}C$/min, $W = 0.3$ g.

and CeO_2 ($d = 16.1$ nm) phases, in accordance with earlier findings [29].

XRD measurements performed on the used 5 wt% Fe/x wt% CeO_2/γ-Al_2O_3 catalysts allowed estimation of the mean Fe_2O_3 particle size (using Scherrer's equation). This was found to be 12.7, 11.5, and 10.5 nm for the 10, 20 and 40 wt% CeO_2-loaded Al_2O_3, respectively.

3.1.3. H_2-TPR studies

Fig. 2 shows H_2-TPR traces in terms of rate of H_2 consumption (μmol-H_2/(g min) versus temperature obtained over the 5 wt% Fe/x wt% CeO_2/γ-Al_2O_3 solids. These traces are largely different than typical H_2-TPR traces of CeO_2 solids [38], possibly due to differences in the extent of interaction between supported CeO_{2-x} crystals and γ-alumina.

The 5% Fe/10% CeO_2/γ-Al_2O_3 solid exhibited three poorly resolved peaks in the 150–800 °C range. The first peak (T_M = 431 °C) was related to the reduction of small CeO_2 crystallites [39], which shifted to higher temperatures with increasing ceria loading. The second peak (T_M = 588 °C) could be attributed to the reduction of CeO_{2-x} microcrystals with greater interaction with γ-alumina [35]. This peak was not clearly distinguished with increased ceria loading to 20 and 40 wt%; instead, a large shoulder developed, apparently also due to the growth of the first and third (T_M = 800 °C) peaks. The high-temperature reduction peak (T_M = 800 °C) appeared in all three solids, associated with the reduction of subsurface oxygen in ceria crystals. The amount of reducible oxygen species due to ceria alone was 395, 700, and 1096 μmol-O/g for the 10, 20, and 40 wt% CeO_2-loaded alumina samples, respectively, after the equivalent amount of O associated with Fe_2O_3 (5 wt% Fe) was subtracted.

Reduction of Fe_2O_3 is known to occur in two (or three) steps via magnetite (Fe_3O_4) or wustite ($Fe_{1-x}O$) [40]. TPR traces of Fe_2O_3 and Au/Fe_2O_3 solids were reported by Munteanu et al. [41] (T_M = 280 and 427 °C). Gillot et al. [42] also confirmed the existence of two peaks in the TPR trace of Fe_2O_3, the positions of which were found to depend on the grain size of iron oxide. Unmuth et al. [43] reported that the H_2-TPR trace of 5 wt% Fe/SiO_2 consisted of two peaks (T_M = 307 and 447 °C), corresponding to a two-step reduction process as mentioned above. In the case of TPR traces shown in Fig. 2, part of the first peak could be assigned to the reduction process $Fe_2O_3 \rightarrow Fe_3O_4$, and part of the second peak could be assigned to the reduction of Fe_3O_4 to Fe^0 [44]. Boudart et al. [45] studied the structure sensitivity of iron in ammonia synthesis in a series of MgO-supported Fe particles and reported full reduction of oxidized iron particles at 427 °C for at least 20 h. The aforementioned reduction characteristics of supported iron oxides are in harmony with the present Mössbauer results, where at the applied H_2 reduction conditions (400 °C, 2 h) only a small fraction of Fe in the sample was fully reduced (see Section 3.1.5).

Table 1
Surface atom composition (%) of the 5 and 10 wt% Fe/50Mg-50Ce-O catalysts derived from XPS analyses

Catalyst	Mg	Ce	Fe	Ce/Mg	Fe/Mg
5% Fe/50Mg-50Ce-O after oxidation[a]	91.4	5.6	3.0		
5% Fe/50Mg-50Ce-O after reduction[b]	93.9	4.4	1.7	0.046	0.018
10% Fe/50Mg-50Ce-O after oxidation[a]	77.3	15.5	7.1		
10% Fe/50Mg-50Ce-O after reduction[b]	78.4	15.2	6.2	0.19	0.079

[a] Oxidation occurred at 800 °C in 20% O_2/He for 2 h.
[b] Reduction occurred at 400 °C in 20% H_2/He for 1 h.

3.1.4. XPS studies

Fig. 3 presents Fe 2p (Fig. 3a) and Ce 3d (Fig. 3b) XPS spectra obtained over the fresh 5% Fe/50Mg-50Ce-O catalyst after H_2 reduction at 400 °C for 1 h. Iron was found in its fully oxidized (Fe^{3+}, 711 eV) state [46,47]. The observed BEs of Ce can be attributed to Ce^{4+}; the observed satellite peaks, to Ce^{3+} [35]. Table 1 reports the surface atom percent composition of x wt% Fe/50Mg-50Ce-O (x = 5, 10) catalysts obtained after the given oxidation and reduction conditions. Reduction of preoxidized 5 and 10 wt% Fe/Mg-Ce-O solids in H_2 at 400 °C resulted in 21 and 2% decreases in Ce surface composition and in 43 and 13% decreases in Fe surface composition (Table 1). The Ce/Mg and Fe/Mg surface ratios obtained after H_2 reduction were about five and four times larger in the case of Mg-Ce-O loaded with 10 wt% compared with 5 wt% Fe. It appears that Fe loading affects the surface enrichment in Ce of ceria crystals. This can be envisioned by considering that Fe_2O_{3-x} is in close contact with ceria crystals, promoting the creation of oxygen vacancies (in the presence of H_2 at 400 °C) by acting as oxygen scavenger. This in turn promotes Ce^{4+} cation diffusion within the ceria lattice toward the surface layers of the solid.

3.1.4.1. Effects of consecutive oxidation/reduction cycles

Fig. 3c presents Fe 2p XPS spectra obtained on the 5% Fe/50Mg-50Ce-O catalyst after consecutive oxidation (800 °C, 20% O_2/He, 3 min) → reduction (25% H_2/He, 650 °C, 10 min) cycles were applied. Table 2 reports surface Ce/Mg, Fe/Mg, and CO_3^{2-}/Mg ratios obtained under the same gas treatments. The following remarks and discussion are appropriate.

Table 2
Surface atom composition (%) of the 5 wt% Fe/50Mg-50Ce-O catalyst derived from XPS analyses after consecutive oxidation → reduction cycles

Cycle	Treatment	Ce/Mg	Fe/Mg	CO_3^{2-}/Mg
1st				
	He[a]	0.068	0.073	0.035
	Oxidation[b]	0.065	0.077	0.018
	Reduction[c]	0.094	0.067	0.014
2nd				
	Oxidation[b]	0.090	0.069	0.016
	Reduction[c]	0.096	0.109	0.015
3rd				
	Oxidation[b]	0.095	0.073	0.015
	Reduction[c]	0.094	0.098	0.012

[a] In He inert atmosphere.
[b] Oxidation occurred at 800 °C in 20% O_2/He for 3 min.
[c] Reduction occurred at 650 °C in 25% H_2/He for 10 min.

(a) After O_2/He treatment, Fe was found in its fully oxidized state (Fe^{3+}, BE=711.1 eV) [46,47]. Treatment in H_2 at 650 °C for 10 min after oxidation at 800 °C for 3 min resulted in partial reduction of Fe^{3+} (711.1 eV) to Fe^{2+} (709.5 eV) [48].

(b) Formation of Fe_3O_4 could be suggested given the coexistence of the two oxidation states of Fe (Fe^{3+}/Fe^{2+}); no Fe^0 (707 eV) [47] was observed. The difficulty in reducing Fe in metal-oxide-supported Fe catalysts is well known (see Section 3.1.3); this difficulty is due to strong metal–support interactions [49], surface decoration effects [50], and formation of chemical compounds [49,51,52]. It has also been reported that the extent of Fe reduction is strongly influenced by the synthesis procedure, pretreatment history, and Fe loading [53]. After oxidation, the BE of Ce is attributed to Ce^{4+} (882.0–882.2 eV), whereas after reduction, the XP spectrum of Ce 3d presented satellite peaks corresponding to Ce^{3+} (as in Fig. 3b).

(c) The Ce/Mg surface ratio appeared lower after the first and second oxidations compared with that after reduction, whereas for the third redox cycle, the Ce/Mg ratio exhibited similar values after oxidation and reduction. This behavior can be explained by considering that some changes in CeO_2 and MgO crystallite sizes may have occurred during the applied redox cycles.

(d) The Fe/Mg surface atom ratio appeared to be lower in reductive conditions than in oxidative conditions for the first

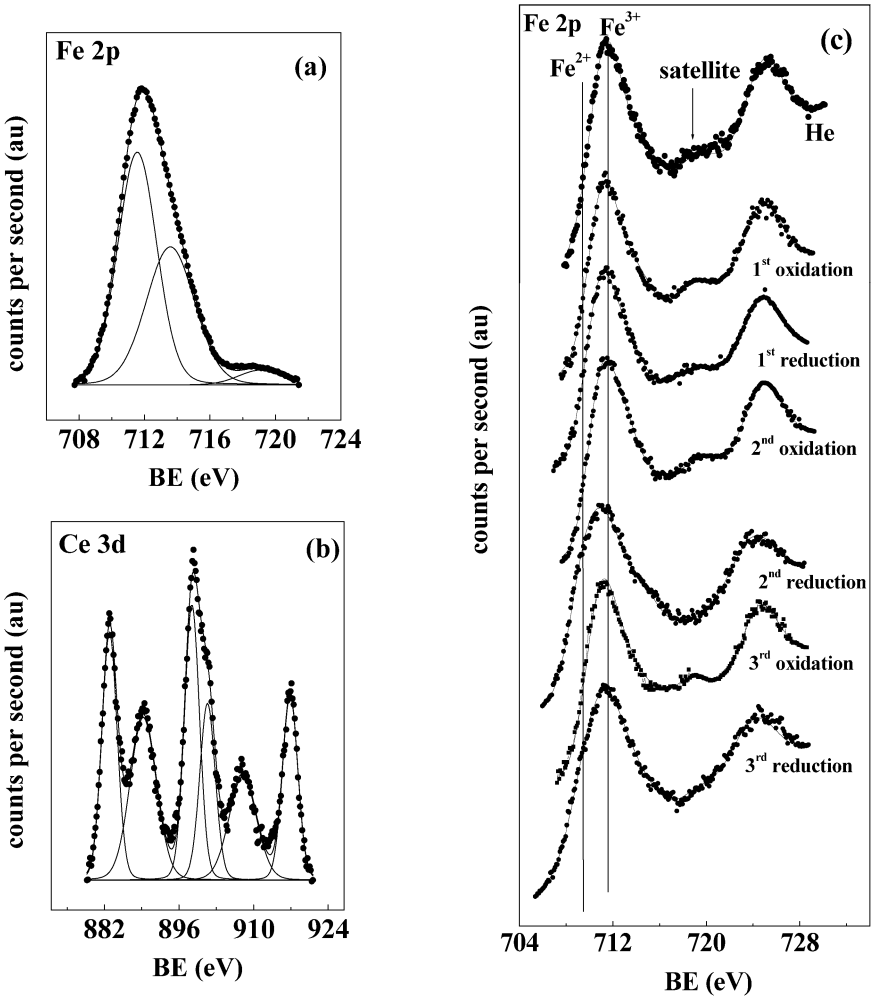

Fig. 3. X-Ray photoelectron spectra obtained on the 5 wt% Fe/50Mg-50Ce-O catalyst. (a) Fe 2p core level after H_2 reduction at 400 °C for 1 h, (b) Ce 3d core level after H_2 reduction at 400 °C for 1 h, (c) Fe 2p core level after three consecutive oxidation (20% O_2/He, 800 °C, 3 min) → reduction (25% H_2/He, 650 °C, 10 min) cycles.

redox cycle, whereas this behavior was reversed during the second and third redox cycles. The possibility that Fe dispersion might have been increased to some extent after the second redox cycle may not be excluded. In fact, Tatarchuk and Dumesic [54] illustrated, by combined XPS and conversion electron Mössbauer spectroscopy, the significant morphological transformation of Fe crystallites in H_2 atmosphere above 500 °C over the Fe/TiO_2 catalyst.

(e) The O 1s XP spectrum showed a peak at 530.1 eV attributed to surface O^{2-} species [55,56], whereas the peak at 531.7–531.9 eV can be attributed to carbonate species [55]. The contribution of carbonate O 1s peak appears to be lower after reduction than after oxidation (Table 2), suggesting that under reducing conditions (650 °C), decomposition and/or reaction of carbonates with hydrogen was favored.

3.1.5. ^{57}Fe Mössbauer studies

Fig. 4 shows Mössbauer spectra collected at 77 K for the fresh (after oxidation at 800 °C, followed by H_2 reduction at 400 °C for 2 h) and after used in phenol steam reforming (700 °C, 4 h) 5 wt% $Fe/20CeO_2/\gamma$-Al_2O_3 catalyst. Tables 3 and 4 report the various Mössbauer parameters estimated from the spectra collected at 298, 77, and 4 K and for the various supported Fe catalysts investigated. The followings remarks and discussion are appropriate:

(a) Iron oxides were clearly present in the fresh 5% Fe/20% CeO_2/γ-Al_2O_3 catalyst (∼53% Fe^{3+}; Table 3), as evidenced by the paramagnetic doublets observed in the spectra obtained at 298 and 77 K (not shown here).

(b) After phenol steam reforming, no sextets appeared corresponding to Fe oxides (Fe^{2+} and Fe^{3+}) or Fe^0 (spectra were fitted with Fe^{2+} and Fe^{3+} doublets). The possibility that some of these doublets may correspond to iron oxide nanoparticles cannot be excluded, because they appeared as doublets at 298 and 77 K due to their super paramagnetic behavior. In addition, iron (Fe^{2+} or Fe^{3+}) migration into the γ-Al_2O_3 and/or CeO_2 lattice [57] cannot be excluded under the high-temperature phenol steam reforming conditions used.

(c) The Mössbauer peak area corresponded to the concentration percentage of the species associated with [58–66]. According to Table 3, a decrease in the percentage of Fe^{3+}, followed by a simultaneous increase of Fe^{2+} after phenol steam reforming, was obtained in all three catalysts. In particular, the decreases in Fe^{3+} were found to be 59, 28, and 14% for the Fe/20% MgO/γ-Al_2O_3, Fe/20% CeO_2/γ-Al_2O_3, and Fe/50Mg-50Ce-O catalysts, respectively (based on spectra recorded at 77 K).

(d) Among the fresh catalysts, Fe^0 was observed only in the 5% Fe/Mg-Ce-O, whereas after phenol steam reforming, no Fe^0 was evident (Table 3). The presence of Fe^0 with $\delta = -0.03$ implies an increase in the electronic density of Fe nucleus, which can be attributed to strong electronic interactions between Fe and Mg-Ce-O support. This was not observed for the CeO_2/γ-Al_2O_3 and MgO/γ-Al_2O_3 supports. The presence of Fe^0 in the fresh 5% Fe/Mg-Ce-O solid depended strongly on the H_2 reduction time ($T = 400$ °C) as

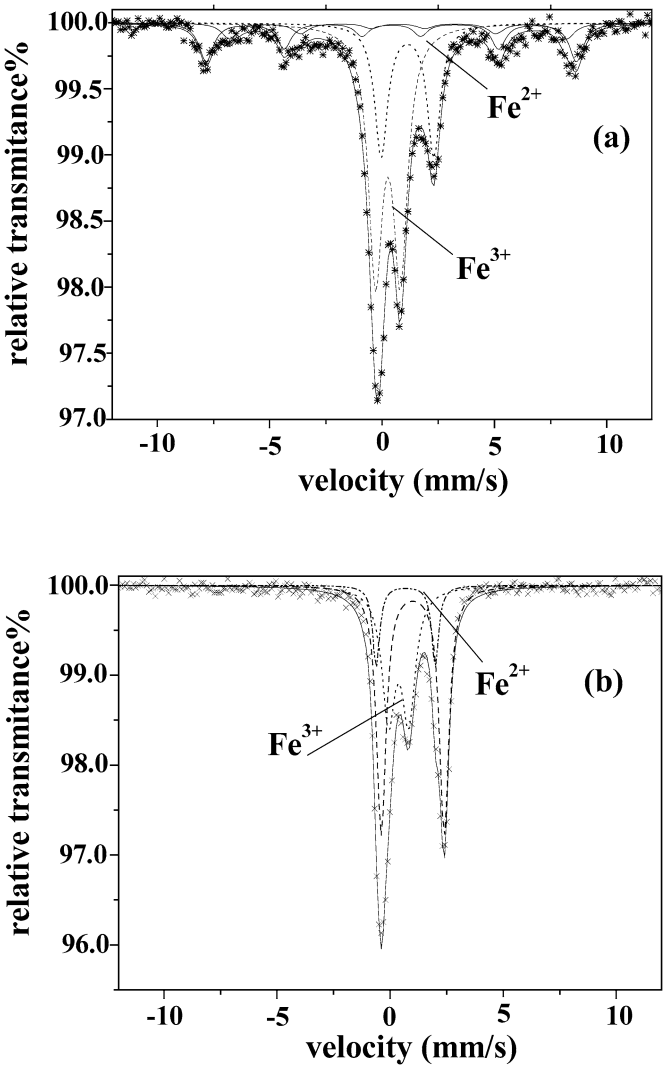

Fig. 4. Mössbauer spectra recorded at 77 K on the 5 wt% Fe/20 wt% CeO_2–Al_2O_3 catalyst as fresh (a), and after phenol steam reforming at 700 °C for 4 h (b).

evidenced by the XPS (1 h; Fig. 3), Mössbauer (2 h; Table 3), and H_2 chemisorption studies (4 h; see Section 3.1.1). These results are consistent in that an increase of reduction time resulted in an increase in the Fe^0 fraction in the solid.

(e) Iron loadings >1 wt% could result in the formation of $MgFe_2O_4$ (spinel phase) in the Fe/MgO system [63]. However, because $MgFe_2O_4$ is ferromagnetic, only a sextet peak must be observed after low-temperature Mössbauer studies. The Mössbauer experiment conducted at 4 K over the 5% Fe/20% MgO/γ-Al_2O_3 catalyst suggested the presence of two components: a paramagnetic doublet attributed to Fe^{2+} and a slightly magnetic component of an intermediate isomer shift corresponding to trivalent and divalent iron with a very low H_f parameter value (see Table 4). These results can be explained as follows. XRD studies performed over the catalyst revealed the presence of $MgAl_2O_4$, suggesting that a significant amount of Mg^{2+} was incorporated into the γ-alumina lattice. Fe is also known to promote the formation of Mg and Al

Table 3
Mössbauer parameters over the 5 wt% Fe/50Mg-50Ce-O, 5 wt% Fe/20CeO_2-Al_2O_3 and 5 wt% Fe/20MgO-Al_2O_3 catalysts (spectra collected at 25 °C)

Catalyst		δ	Γ	DE_Q	H_{hf}	(%)
5% Fe/20MgO/γ-Al_2O_3[a]	Fe^{+3}	0.29	0.67	0.97	0	60.0
	Fe^{+2}	1.14	0.6	2.0	0	17.8
	Fe^{+2}	0.83	0.74	1.74	0	22.2
5% Fe/20MgO/γ-Al_2O_3[b]	Fe^{+3}	0.25	0.5	0.92	0	17.6
	Fe^{+2}	0.76	0.66	1.56	0	46.8
	Fe^{+2}	1.13	0.56	1.62	0	35.6
5% Fe/20CeO_2/γ-Al_2O_3[a]	Fe^{+3}	0.33	0.68	0.96		52.5
	Fe^{+2}	1.05	0.78	2.0		23.7
	$Fe^{+\delta}$ [c]	0.56	0.36	1.88		3.8
	$Fe^{+\delta}$ [c]	0.52	0.56	0	446	20.0
5% Fe/20CeO_2/γ-Al_2O_3[b]	Fe^{+3}	0.26	0.64	1.1	0	32.4
	$Fe^{+\delta}$ [c]	0.74	0.6	1.72	0	30.2
	Fe^{+2}	1.13	0.64	1.78	0	37.4
5% Fe/Mg-Ce-O[a]	Fe^{+3}	0.36	0.58	0.8	0	40.5
	Fe^{+2}	1.06	0.5	0.88	0	47.6
	a-Fe	−0.03	0.3	0	330	11.8
5% Fe/Mg-Ce-O[b]	Fe^{+3}	0.45	0.55	1.0	0	34.9
	Fe^{+2}	1.03	0.48	0.48	0	65.1

[a] After oxidation in 20% O_2/He at 800 °C followed by reduction in 20% H_2/He at 400 °C for 2 h (fresh catalyst).
[b] After phenol steam reforming reaction at 700 °C for 4 h.
[c] Indicates unknown oxidation state based on the Mössbauer measurements at 25 °C.

Table 4
Mössbauer parameters over the 5 wt% Fe/20CeO_2-Al_2O_3 and 5 wt% Fe/20MgO-Al_2O_3 catalysts (spectra collected at 77 and 4 K)

Catalyst		δ	Γ	DE_Q	H_{hf}	(%)
5% Fe/20MgO/γ-Al_2O_3[a]	Fe^{+3}	0.33	0.7	1.1	0	60.8
(77 K)	Fe^{+2}	1.22	0.62	2.36	0	39.2
5% Fe/20MgO/γ-Al_2O_3[b]	Fe^{+3}	0.49	0.78	0.8	0	24.8
(77 K)	Fe^{+2}	1.04	0.58	2.5	0	49.7
	Fe^{+2}	1.05	0.32	3.0	0	25.5
5% Fe/20CeO_2/γ-Al_2O_3[a]	Fe^{+3}	0.37	0.75	1.1	0	50.8
(77 K)	Fe^{+2}	1.24	0.7	2.34	0	25.6
	Fe^{+2}	0.82	0.86	0	467	7.6
	Fe^{+3}	0.52	0.64	0	513	16
5% Fe/20CeO_2/γ-Al_2O_3[b]	Fe^{+3}	0.48	0.7	0.88	0	36.4
(77 K)	$Fe^{+\delta}$ [c]	0.79	0.36	2.6	0	12.3
	Fe^{+2}	1.1	0.5	1.4	0	51.3
5% Fe/20MgO/γ-Al_2O_3[b]	Fe^{+3}	0.37	0.6	0.9	0	9
(4 K)	Fe^{+2}	1.05	0.6	3	0	49
	$Fe^{+2,+3}$	0.84	0.62	1.74	144	42

[a] After oxidation in 20% O_2/He at 800 °C followed by reduction in 20% H_2/He at 400 °C for 2 h (fresh catalyst).
[b] After phenol steam reforming reaction at 700 °C for 4 h.
[c] Indicates unknown oxidation state based on the Mössbauer measurements at 77 K.

mixed spinel phases, which are characterized by high concentrations of structural defects [67]. Therefore, the spinel phase of $Mg_{1-x}Fe^{(II)}_{x-3a}Fe^{(III)}_{2a}[\ ]Al_2O_4$ (where [ ] is a defect site) could be proposed as a component of the 5% Fe/20% MgO/γ-Al_2O_3 catalyst. This spinel oxide is ferromagnetic and should appear as sextet in Mössbauer spectra when Fe is present in sufficient amounts. In the present case, apparently the 5 wt% Fe content led to a poorly resolved sextet with a low value of H_f. Moreover, the presence of Fe^{+2} and Fe^{+3} in the lattice resulted in an intermediate isomer shift of 0.84 for this component (Table 4).

(f) The 5% Fe/20% MgO/γ-Al_2O_3 catalyst (Table 3) showed chemical shift ($\delta = 1.13$) and quadrupole splitting ($\Delta E_Q = 1.62$) corresponding to Fe^{2+} in the oxide lattice, indicating partial reduction of Fe_2O_3 into FeO under reaction conditions.

(g) Iron species with $\delta = 0.32$ and $\Delta E_Q = 1.18$ mm/s can be attributed to Fe^{3+} in a relatively strong interaction with γ-Al_2O_3 support [62]. According to the Mössbauer parameters given in Tables 3 and 4, the 5% Fe/20% CeO_2/γ-Al_2O_3 and 5% Fe/20% MgO/γ-Al_2O_3 catalysts after oxidation followed by reduction and after steam reforming have an iron component (Fe^{3+}) with Mössbauer parameters very close to those previously mentioned.

3.2. Catalytic performance of supported Fe catalysts

3.2.1. Effect of support chemical composition

Fig. 5 presents results of the H_2 product concentration (mol%) obtained at 600, 650, and 700 °C after steady state was achieved (30 min on reaction stream) over six supported Fe catalysts (5 wt% Fe) of varying support compositions. The 10CeO_2-Al_2O_3 (1), 10MgO-Al_2O_3 (2), 20CeO_2-Al_2O_3 (3), and 20MgO-Al_2O_3 (4) supports were prepared by the incipient wetness impregnation method (see Section 2.1). Support (5) is commercial γ-alumina, and support (6) is 50Mg-50Ce-O, a mixed metal oxide (MgO, CeO_2) prepared by the sol–gel method (see Section 2.1). The maximum theoretical H_2 concentration expected given the network of reactions (2) and (3), the feed gas composition used, and considering 100% phenol conversion was 4.4 mol% H_2.

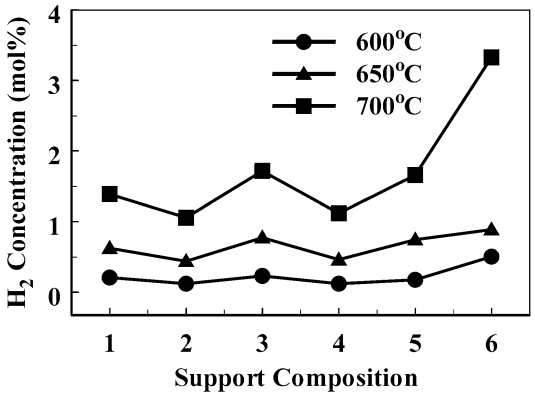

Fig. 5. Dependence of H_2 product concentration (mol%) on support chemical composition and reaction T obtained over (1) 5 wt% Fe/10 wt%CeO_2-Al_2O_3; (2) 5 wt% Fe/10 wt% MgO-Al_2O_3; (3) 5 wt% Fe/20 wt% CeO_2-Al_2O_3; (4) 5 wt% Fe/20 wt% MgO-Al_2O_3; (5) γ-Al_2O_3; (6) 5 wt% Fe/50Mg-50Ce-O catalysts. Reaction conditions: 0.25% C_6H_5OH/20% H_2O/He; $t = 30$ min; $W = 0.15$ g; $F_T = 100$ NmL/min; GHSV ≈ 80,000 h^{-1}.

Table 5
Catalytic performance of various supported-Fe catalysts for the phenol steam reforming (0.25% C_6H_5OH/20% H_2O/He) after 30 min on stream at $T = 700\,^{\circ}C$

Catalyst	H_2 (mol%)	CO (mol%)	CO_2 (mol%)	X (%)	S_{H_2} (%)	Carbon (μmol-C/g)
5Fe/10MgO-Al_2O_3	1.06	4.56×10^{-1}	1.93×10^{-1}	33.8	23.7	440
5Fe/20MgO-Al_2O_3	1.12	3.59×10^{-1}	3.0×10^{-1}	35.2	25.7	429
5Fe/10CeO_2-Al_2O_3	1.39	5.07×10^{-1}	5.03×10^{-1}	40.5	31.6	355
5Fe/20CeO_2-Al_2O_3	1.72	4.07×10^{-1}	7×10^{-1}	59.1	39.3	287
5Fe/40CeO_2-Al_2O_3	2.3	4.55×10^{-1}	9.2×10^{-1}	61	45.8	167
5Fe/50Mg-50Ce-O	3.2	2.53×10^{-1}	1.03	63.3	54.3	260
5Fe/Al_2O_3	1.09	6.09×10^{-1}	3.82×10^{-1}	48.2	34.3	448

Table 5 presents results of the reaction gas product analysis, the phenol conversion (X, %), the H_2 reaction selectivity (S_{H_2}, %), and the amount (μmol-C/g) of accumulated carbon-containing species (termed "carbon") measured after 30 min of reaction at 700 °C. The "carbon" amount was measured by a transient isothermal titration experiment with 20% H_2O/He as reported recently [28,29]. No CH_4 or higher hydrocarbons were measured besides small amounts of benzene (use of HPLC). For the latter component, the corresponding phenol conversion was estimated to be <5%. These results support the reaction scheme described previously (see Section 2.3). The following discussion is offered in an attempt to explain the role of support composition on the catalytic behavior of supported Fe solids (Fig. 5 and Table 5).

3.2.1.1. x wt% CeO_2–Al_2O_3 versus x wt% MgO–Al_2O_3

5 wt% Fe supported on x wt% CeO_2–Al_2O_3 solids exhibit better catalytic performance in terms of phenol conversion, hydrogen selectivity, and yield (mol%) compared with the same amount of iron supported on x wt% MgO–Al_2O_3 solids. According to XRD studies (see Section 3.1.2), the spinel phase of $MgAl_2O_4$ was detected in the latter catalytic systems, where it was reported to be practically inactive in steam reforming reactions [68]. Furthermore, based on the Mössbauer studies presented and discussed previously (Section 3.1.5), the spinel phase of $Mg_{1-x}Fe^{(II)}_{x-3a}Fe^{(III)}_{2a}[\ ]Al_2O_4$ was suggested to be part of the Fe/MgO–Al_2O_3 catalyst composition. In addition, Sanchez and Gazquez [66] reported that CeO_2 did not favor penetration of Fe into the ceria-promoted alumina support. It can be speculated whether the higher percentage of Fe^{3+} in the Fe/x wt% CeO_2/γ-Al_2O_3 solids compared with Fe/x wt% MgO/γ-Al_2O_3 (see Tables 3 and 4) under phenol steam reforming could be one reason for their higher activity toward H_2 formation.

It has been recently reported [69] that MgO and CeO_2 contribute significantly to steam reforming of the phenol reaction path through –OH and/or H back-spillover onto the iron/iron oxide surfaces. It is known that γ-Al_2O_3 has a large reservoir of hydroxyl groups that favors their back-spillover or that of adsorbed water to the metal surface of M (or MO_x)/γ-Al_2O_3 catalysts [70].

The aforementioned factors support the view that the amount of active sites in both iron oxide (see Section 3.1.5) and MgO-Al_2O_3 phases might be lower for Fe/x wt% MgO-Al_2O_3 than for Fe/x wt% CeO_2-Al_2O_3. A precise quantification of the extent of decrease of the iron oxide and support active sites in the former catalytic systems compared with the latter cannot be done from the results of the present work, however.

According to the results reported in Table 5, the amount of accumulated "carbon" on Fe/10MgO-Al_2O_3 at 700 °C is about 24% greater than that deposited on Fe/10CeO_2-Al_2O_3. Moreover, at 600 °C (not presented in Table 5), the amount of accumulated "carbon" was 55% greater on the former than on the latter (790 vs. 510 μmol-C/g). Similar behavior was seen for the Fe/20MgO-Al_2O_3 and Fe/20CeO_2-Al_2O_3 catalysts (Table 5). These important results provide evidence that CeO_2-Al_2O_3 more strongly facilitates gasification by steam of carbonaceous deposits toward CO, CO_2, and H_2, thus explaining the H_2 product yield (mol%) behavior shown in Fig. 5.

Basicity measurements obtained over the 20% MgO/γ-Al_2O_3, γ-Al_2O_3, and 20% CeO_2/γ-Al_2O_3 supports showed that the latter exhibited the largest specific amount of basic sites (1.33 μmol/m^2) compared with the other two supports (0.80 μmol/m^2 for 20% MgO/γ-Al_2O_3 and 0.76 μmol/m^2 for γ-Al_2O_3). This result, together with the BET values of the three solids (see Section 3.1.1), is in harmony with the activity results shown in Fig. 5, where enhanced support basicity would be expected to result in increased water chemisorption, thereby leading to enhanced gasification of deposited "carbon" [71], as well as of the rate of –OH and/or H back-spillover [69].

According to the H_2-TPR results of Fig. 2 (and other results not reported here), the amount of reducible oxygen species at 100–800 °C for the Fe/20CeO_2-Al_2O_3 and Fe/20MgO-Al_2O_3 catalysts were 700 and 438.9 μmol-O/g, respectively. Similarly, for the Fe/10CeO_2-Al_2O_3 and Fe/10MgO-Al_2O_3 catalysts, the amount of reducible oxygen species was 394 and 360 μmol-O/g, respectively. According to recent investigations [69], labile oxygen species are likely important intermediate species of the steam reforming of phenol over MgO- and CeO_2-supported Rh catalysts; therefore, these findings could provide additional explanations for the higher H_2 product yields obtained on CeO_2-Al_2O_3-supported compared with MgO-Al_2O_3-supported Fe catalysts.

3.2.1.2. Superiority of the 50Mg-50Ce-O support According to the catalytic results reported in Table 5, iron supported on the mixed oxide 50Mg-50Ce-O prepared by the sol–gel method exhibited by far the highest H_2 yield of the supported Fe catalysts. In what follows, the main factors supported by the present work

that reasonably explain the catalytic performance of the 5 wt% Fe/50Mg-50Ce-O catalyst are discussed.

Based on the Mössbauer studies (Tables 3 and 4) conducted over the fresh Fe/50Mg-50Ce-O, Fe/20CeO_2-Al_2O_3, and Fe/20MgO-Al_2O_3 catalysts (after H_2 reduction at 400 °C for 2 h), only the Fe/50Mg-50Ce-O solid exhibited a small fraction of iron in the metallic state (Fe^0), which under phenol steam reforming was converted to Fe^{2+} and Fe^{3+}. As discussed later (Section 3.2.4), a 10-min reduction in H_2 at 650 °C after oxidation at 800 °C gave significantly higher H_2 product rates than would have been obtained had reduction not been performed over the 5 wt% Fe/Mg-Ce-O catalyst. It can be speculated that the reduction of supported Fe^{3+} to Fe^{2+} is favored when Mg-Ce-O is used as an iron support rather than one of the other metal oxides investigated. In fact, the quadrupole-splitting variation of the Fe^{2+} doublet reported in Table 3 for the various supported Fe catalysts (same Fe loading, 5 wt%) indicates a significant variation in iron concentration in the local environment of Fe^{2+}. This would be expected to have an influence on the local surface Fe^{2+} environment.

As already discussed for the MgO-Al_2O_3 and CeO_2-Al_2O_3 supports, the surface basicity of the support plays an important role in the phenol steam reforming reaction. The amount of basic sites determined for the 50Mg-50Ce-O support was found to be 0.91 μmol/m^2 or 73 μmol/g. This is the second largest amount among the supports presented in Fig. 5, behind only that of the 20CeO_2-Al_2O_3 solid (1.33 μmol/m^2 or 86 μmol/g). The fact that Fe/50Mg-50Ce-O exhibited a 85% greater H_2 product yield (mol% H_2) than Fe/20CeO_2-Al_2O_3 (with the latter having 18% more basic sites (μmol/g)), suggests that support surface basicity alone cannot account for the significantly enhanced of phenol steam reforming activity toward H_2 formation.

The Fe/50Mg-50Ce-O catalyst exhibited the largest amount (747 μmol O/g) of reducible oxygen species among the supports (Fig. 5) according to a similar H_2-TPR experiment presented in Fig. 2. This amount is only 7% larger than that for the 20CeO_2-Al_2O_3 and 32% less than that for the 40CeO_2-Al_2O_3 support. However, the amount of easily reducible oxygen species (in the 150–500 °C range) in the 50Mg-50Ce-O solid was 25% greater than that for 20CeO_2-Al_2O_3 and 18% greater than that for 40CeO_2-Al_2O_3. In addition, the amount of "carbon" deposits on Fe/50Mg-50Ce-O at 700 °C was 10% lower than that for Fe/20CeO_2-Al_2O_3 and 6% greater than that for Fe/40CeO_2-Al_2O_3 (Table 5). These findings suggest that labile oxygen and/or –OH species of Mg-Ce-O support partly determine the activity of supported Fe catalysts under phenol steam reforming reaction conditions through a back-spillover process, as reported previously [69].

3.2.1.3. Effects of ceria loading (Fe/x wt% CeO_2-Al_2O_3) Here we discuss the effects of ceria loading on the catalytic activity of Fe/x wt% CeO_2-Al_2O_3 based on the results of the present work. Table 5 shows that increasing the amount of deposited CeO_2 on alumina from 10 to 40 wt% resulted in significantly increased H_2 product yield (by 65%) and phenol conversion. At the same time, the CO/CO_2 product ratio decreased by a factor of two, whereas the amount of deposited "carbon" (μmol-C/g) also decreased significantly (by 30%; see Table 5). Furthermore, the amount of reducible oxygen species in x wt% CeO_2-Al_2O_3 supports increased significantly with increasing ceria loading (see Section 3.1.3). These results clearly illustrate the important role of labile oxygen present in ceria to promote "carbon" gasification, as well as the water–gas shift reaction [72].

It also has been reported [35,73] that stabilization of γ-alumina against thermal sintering is promoted by ceria, which could lead to an increase in Fe dispersion [35,74]. However, the Fe_2O_3 particle size determined by XRD on the used 5 wt% Fe/x wt% CeO_2/Al_2O_3 solids ($x = 10$, 20, and 40) was found to differ by only 17% (see Section 3.1.2). Therefore, the catalytic results presented in Fig. 5 and Table 5 are due mainly to the reasons discussed in the previous paragraph. It has been reported that partially reduced CeO_x entitites ($x < 2$) are able to migrate onto metal particles (M/CeO_2 system), thus blocking active sites [75]. This migration cannot be excluded in the present catalytic system; if this did occur, it would be favored over the smaller CeO_2 crystallites (the case of Fe/10% CeO_2-Al_2O_3).

3.2.1.4. CO/CO_2 product ratio The CO/CO_2 product ratio obtained at 700 °C for the seven different supports (Table 5) was found to be in the 0.24–2.4 range, a difference of an order of magnitude. This indicates the strong effect of the support on the rates of reactions (2) and (3), which control the overall H_2, CO, and CO_2 product yields. The fact that the 50Mg-50Ce-O support exhibits the largest hydrogen product yield (mol% H_2) and the lowest CO/CO_2 product ratio (Fig. 5 and Table 5) supports the view that this particular support composition largely promotes the WGS reaction (3).

3.2.2. Effects of iron loading (x wt% Fe/Mg-Ce-O)

Fig. 6a shows the effect of Fe loading of x wt% Fe/50Mg-50Ce-O catalysts on the H_2 integral specific reaction rate (μmol-H_2/(g s)) after 30 min on reaction stream at 600, 650, and 700 °C. It is seen that reaction rate went through a maximum at the Fe loading of 5 wt% for all three reaction temperatures studied. Note that H_2 production arises from both reactions (2) and (3) (see Section 2.3), and thus the plotted H_2 reaction rate is the sum of the rates in the given network of reactions involved in the steam reforming of phenol.

Fig. 6b reports the amount of "carbon" deposited (see Section 3.2.1) on each of the four supported Fe catalysts investigated at 600 and 700 °C after 30 min of phenol steam reforming. It is shown that as Fe loading increased, "carbon" accumulation on the catalyst surface also increased. This increase appears to be significant when Fe loading increased from 5 to 10 wt% and at the highest temperature of 700 °C (Fig. 6b).

Based on the results of Figs. 6a and b, it could be argued that a monotonic increase in an important parameter that largely affects reaction rate with increasing Fe loading can justify the existence of a maximum in the H_2 reaction rate versus Fe loading relationship (Fig. 6a). This is so because the reaction rate is expected to be inversely proportional to the amount of de-

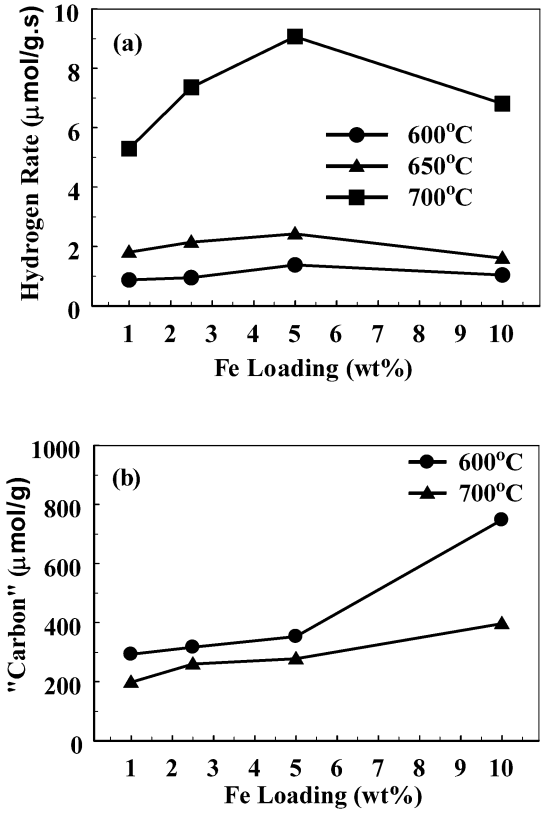

Fig. 6. Dependence of (a) hydrogen integral specific reaction rate (μmol-H_2/(g s)), and (b) "carbon" deposition on Fe loading (wt%) and reaction temperature for the Fe/50Mg-50Ce-O catalyst. Reaction conditions: 0.25% C_6H_5OH/20% H_2O/He; $t = 30$ min; $W = 0.15$ g; $F_T = 100$ NmL/min; GHSV ≈ 80,000 h^{-1}.

posited carbon. According to the preceding discussion about the role of Fe^{2+} on catalyst activity (see also Section 3.2.4), it could be stated that if the Fe^{2+} surface concentration increased monotonically with increasing Fe loading, then this along with the relationship of deposited "carbon" versus Fe loading observed (Fig. 6b) could provide a way to reasonably understand the catalytic activity results in Fig. 6a.

3.2.3. Comparison with a commercial Ni-based catalyst

Table 6 reports reaction gas product composition (mol%), phenol conversion, H_2 reaction selectivity, and "carbon" deposition after 30 min on reaction stream in the 600–750 °C range over a commercial nickel catalyst (44 wt% NiO/γ-Al_2O_3, Süd-Chemie, code C11-PR) used in tar steam reforming reactions. It also reports similar results for the 5 wt% Fe/50Mg-50Ce-O catalyst. The commercial catalyst exhibited superior H_2 product yield (mol%) and selectivity compared with the Fe/Mg-Ce-O catalyst, but a similar amount of deposited "carbon," at 600 and 650 °C. However, at the highest reaction temperature of 700 °C, the commercial catalyst exhibited only 20% more H_2 yield than the Fe/Mg-Ce-O catalyst and a similar amount of deposited "carbon."

Results of the H_2-specific integral production rate (per g of metal) and conversion of the WGS reaction in the 600–700 °C range are presented in Figs. 7a and b, respectively, for the two catalytic systems. The Ni-based catalyst exhibited greater specific activity than the Fe/Mg-Ce-O catalyst at 600 and 650 °C, but lower (by a factor of 2.5) at 700 °C. In contrast, the Fe-based catalyst had a greater (by 15–20 percentage units) CO conversion (WGS reaction), in good agreement with the literature [10]. The CO/CO_2 product ratios for the 5 wt% Fe/Mg-Ce-O and Ni-based commercial catalyst were 0.24 and 10.3 at 700 °C and 0.52 and 1.25 at 600 °C. These are important findings in terms of the practical application of steam reforming of organic molecules to produce H_2 gas of low CO content for use in fuel cells. The lower the CO content the less hydrogen gas will be consumed in a subsequent methanation catalytic reactor ($CO/H_2 \rightarrow CH_4 + H_2O$), and thus the less carbon should be formed on the catalyst surface (deactivation phenomenon).

The results of Table 6 and Fig. 7 suggest that the 5 wt% Fe/50Mg-50Ce-O catalyst developed in the present work could be further considered and studied for practical use in tar steam reforming reactions in fluidized-bed reactors as an alternative to Ni-based catalysts, because nickel mass loss in the environment during operation of such reactors must be avoided due to toxicity concerns.

Table 6
Catalytic performance of DOLII, Ni-commercial, Fe/50Mg-50Ce-O and 50Mg-50Ce-O solids for the phenol steam reforming (0.25% C_6H_5OH/20% H_2O/He) after 30 min on stream in the 600–700 °C range

Catalyst	T (°C)	H_2 (mol%)	CO (mol%)	CO_2 (mol%)	X (%)	S_{H_2} (%)	Carbon (μmol-C/g)
35 wt% Ni/γ-Al_2O_3 (commercial)	600	3.18	0.76	0.61	70	71.4	361
	650	3.59	1.81	0.10	78	80.7	345
	700	3.86	1.77	0.17	84.3	87.2	285
DOLII	600	0.17	0.04	0.05	2.2	2.9	480
	650	0.73	0.08	0.13	14.3	12.3	440
	700	1.83	0.45	0.58	36	30.9	428
5 wt% Fe/Mg-Ce-O	600	0.51	0.08	0.15	2.5	8.9	353
	650	0.8	0.13	0.25	30.4	14.0	320
	700	3.2	0.25	1.03	63.3	54.3	260
50Mg-50Ce-O	600	0.015	0.004	0.005	0.1	0.3	–[a]
	650	0.05	0.012	0.016	1.8	1.7	–[a]
	700	0.118	0.028	0.038	2.3	1.9	–[a]

[a] Not measured.

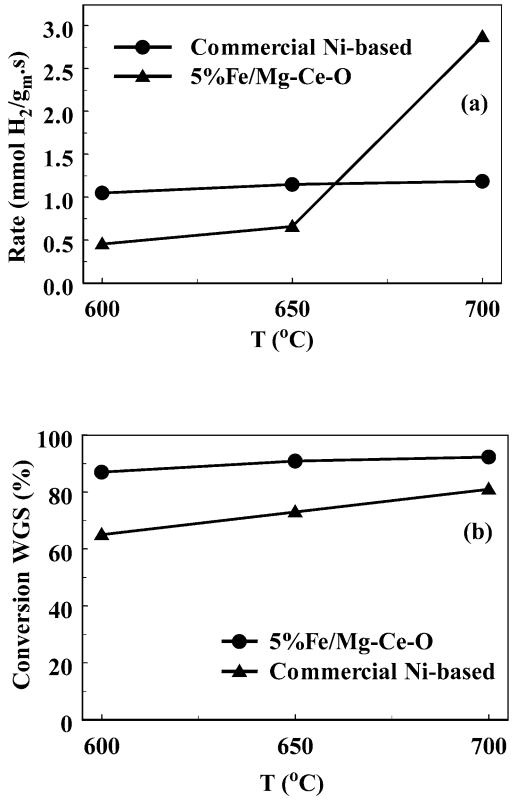

Fig. 7. Comparison of (a) hydrogen integral specific reaction rate (mmol-$H_2/(g_m\,s)$), and (b) conversion of water–gas shift reaction obtained in the 600–700 °C range between 5 wt% Fe/50Mg-50Ce-O and commercial Ni-based (C11-PR, Süd-Chemie) catalysts. Reaction conditions: 0.25% C_6H_5OH/20% H_2O/He; $t = 30$ min; $W = 0.15$ g; $F_T = 100$ NmL/min; GHSV $\approx 80{,}000\ h^{-1}$.

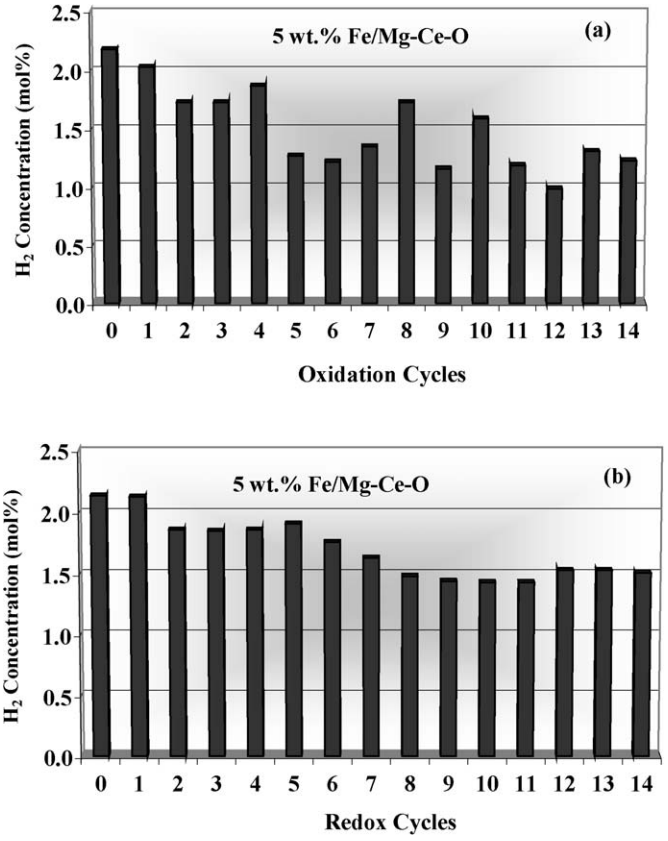

Fig. 8. H_2 product concentration (mol%) obtained after consecutive (a) oxidation → reaction, and (b) oxidation → reduction → reaction cycles for short times at 650 °C over the 5 wt% Fe/50Mg-50Ce-O catalyst. Reaction feed gas: 0.25% C_6H_5OH, 20% H_2O, He balance gas; oxidation step: air at 800 °C for 3 min; reduction step: 25% H_2/He at 650 °C for 10 min; reaction step, 5 min.

3.2.4. Stability of 5 wt% Fe/Mg-Ce-O catalyst under consecutive reaction cycles

As pointed out in the Introduction, the present work was motivated by the AER process used in a fast-recycled fluidized-bed reactor [26,27], in which in about 3–5 min the catalytic bed material is transformed from the reaction zone to the combustion one for regenerating the CO_2 absorbent material and burning the accumulated "carbon" deposits. Thus, it was important to test the phenol steam reforming activity of the 5% Fe/50Mg-50Ce-O catalyst under consecutive *oxidation → reaction*, and *oxidation → reduction → reaction* cycles.

Fig. 8a compares the H_2 product concentration obtained after consecutive *oxidation → reaction* cycles at 650 °C (with oxidation performed with air at 800 °C for 3 min). The cycle numbered 0 in Fig. 8 refers to the activity of the catalyst before the first cycle was applied. The activity of the catalyst decreased with increasing *oxidation → reaction* cycles (Fig. 8a); in particular, the initial activity dropped by about 50% after 14 consecutive cycles. However, after the sixth cycle, the catalyst activity remained practically the same.

Fig. 8b compares the H_2 product concentration obtained after consecutive *oxidation → reduction → reaction* cycles at 650 °C (with reduction performed with a 25% H_2/He gas mixture for 10 min). The deactivation thus obtained accounted for only 25% (based on the 14th cycle), considerably less than that obtained under the *oxidation → reaction* cycles (Fig. 8a). The effect of H_2 reduction at 650 °C was to increase the initial fraction of iron (III) oxide reduction to Fe^{2+}/Fe^0, according to the work of Boudart et al. [45] on Fe/MgO, a result that seems to enhance phenol steam reforming to H_2 formation for the first 5 min of the reaction. It is speculated that the *oxidation → reduction → reaction* cycles also better promote favorable iron/iron oxide particle morphologies compared with the *oxidation → reaction* cycles, a phenomenon that also may affect catalytic activity. This is a fundamental aspect that merits further investigation.

According to the XPS results (Fig. 3), after the first oxidation, the oxidation state of Fe was that of Fe^{3+}, whereas after reduction, 13% of the surface Fe^{3+} was reduced to Fe^{2+}. The Fe^{3+} reduction increased by 13, 21, and 23% after the first, second, and third *oxidation → reduction* cycles, respectively. These results are in agreement with the stabilization of iron in the 2+ oxidation state during the phenol steam reforming reaction according to the Mössbauer studies (Table 3).

The presence of carbonate species on the catalyst surface was evidenced by XPS, where during *oxidation → reduction* cycles their concentration decreased to a greater extent under reducing conditions than under oxidizing conditions. This decrease could be related to the observed catalyst deactivation (Fig. 8), given the fact that carbonates may hinder to some ex-

tent the back-spillover of oxygen/OH species from the support to the metal [76], an essential step in phenol steam reforming [69].

3.3. Catalytic performance of natural materials

Haematite and olivine ($(Mg, Fe)_2SiO_4$) were investigated in the present work for their catalytic activity toward phenol steam reforming. Both solids were calcined in air at 800 °C for 2 h, and haematite was also reduced in pure H_2 at 400 °C for 2 h before the catalytic measurements. These materials appeared to be practically inactive at reaction temperatures below 700 °C (H_2 (mol%) < 0.4; Fig. 9a). At 700 °C, olivine had a higher H_2 yield than haematite, likely due to the presence of MgO in the olivine, which is known to promote tar steam reforming [77–79]. On the other hand, both materials had significantly lower H_2 yields (10 and 30 times lower, respectively) than the 5% Fe/50Mg-50Ce-O catalyst at 700 °C (Fig. 9a).

The four natural CO_2 absorbent materials (calcites and dolomites), with the exception of DOLII, were practically inactive at 600 °C (Fig. 9b). The dolomites exhibited better catalytic activity than the calcites at 650 and 700 °C, whereas DOLII appeared to be better than D4, a result in agreement with their exposed surface areas (12.4 vs. 6.4 m^2/g). Table 6 presents the catalytic performance of DOLII in the 600–700 °C range. At 700 °C, a H_2 concentration of 1.83 mol% was obtained, compared with 3.2 mol% for 5% Fe/50Mg-50Ce-O (Table 5). The catalytic activity results shown in Fig. 9b suggest that DOLII behaved better than calcites, due to the stabilizing effect of MgO against sintering of CaO [80]. DOLII had a significantly higher amount of "carbon" deposits on the surface than did Fe/Mg-Ce-O (see Table 6).

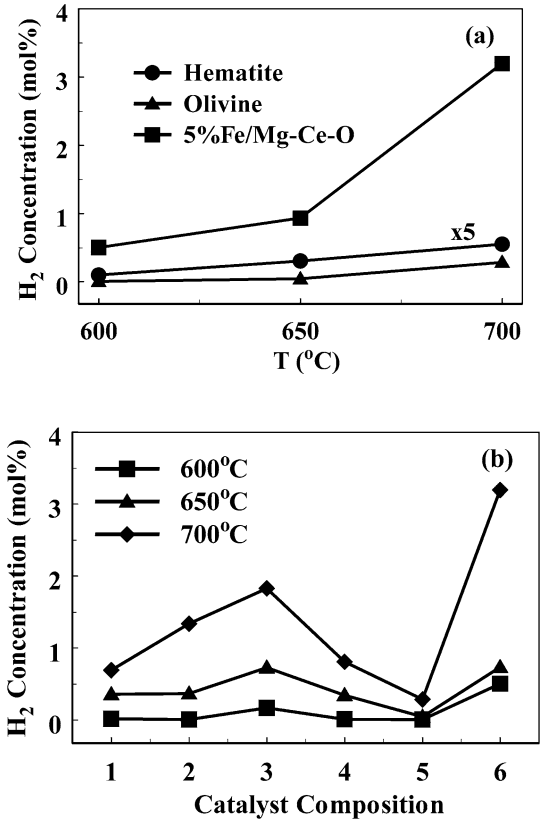

Fig. 9. H_2 product concentration (mol%) obtained over (a) 5 wt% Fe/50Mg-50Ce-O, hematite, and olivine, and (b) natural materials: calcites (1), (4); dolomite D4 (2), and DOLII (3); olivine (5). For comparison, the 5 wt% Fe/50Mg-50Ce-O catalyst (6) is also shown. Reaction conditions: 0.25% C_6H_5OH/20% H_2O/He; $t = 30$ min; $W = 0.15$ g; $F_T = 100$ NmL/min; GHSV ≈ 80,000 h^{-1}.

3.4. Mechanistic aspects of phenol steam reforming over supported and nonsupported Fe catalysts

Scheme 1 provides the essentials of the mechanisms proposed in the literature for the steam reforming of phenol and of similar to phenol molecules over metal oxides, including the natural materials, MgO, and iron oxides (Fe/Mg-Ce-O catalyst) used in the present work. Adsorption of phenol onto a metal oxide surface is the result of interaction of the π-electron system and the aromatic –OH group with two adjacent surface hydroxyl groups (Scheme 1a). The latter are populated on the metal oxide surface via a H_2O dissociative chemisorption step during the steam reforming reaction. This dual site adsorption mechanism has been proposed for the adsorption of chlorobenzene on the surface of ZnO [81] and by Corella et al. [79] for the steam reforming of phenathrene (tar species). Pohle [82] suggested that on silica with a high concentration of surface hydroxyls, fluorobenzene can be retained in a dual adsorption site such that interaction of fluorine atoms with surface OH groups (hydrogen bonding) and the interaction of π-electrons of the aromatic ring with surface OH groups contribute to adsorption of the organic molecule. Opening of the benzene ring by this adsorption mode leads to several successive elementary steps toward formation of H_2, CO, CO_2, and other adsorbed C_xH_y species ("carbon" deposits) [79].

Scheme 1b shows the adsorption mode of phenol on the iron oxides surfaces [83] for the present Fe/Mg-Ce-O catalytic system, where under steam reforming the predominant phases of iron are those of Fe_2O_3 and FeO. Phenol is adsorbed dissociatively on the iron oxide surface to form surface phenoxy species [84], a type of bonding that is much stronger than the bonding between water and iron oxide, and is not replaced by water [83]. The derived hydrocarbon fragments from the phenoxy adsorbed species are oxidized by labile O and/or –OH species of support via a back-spillover process [69], and by –OH groups residing on iron oxides surfaces to form H_2, CO, and CO_2 (bifunctional catalysis; see Scheme 1b).

According to the catalytic results given in Table 6, the contribution of Mg-Ce-O support alone via the dual-site mechanism presented in Scheme 1a is minor compared with the Fe/Mg-Ce-O catalytic surface (Scheme 1b). Finally, it should be noted that the WGS reaction also occurs, further contributing to H_2 and CO_2 formation.

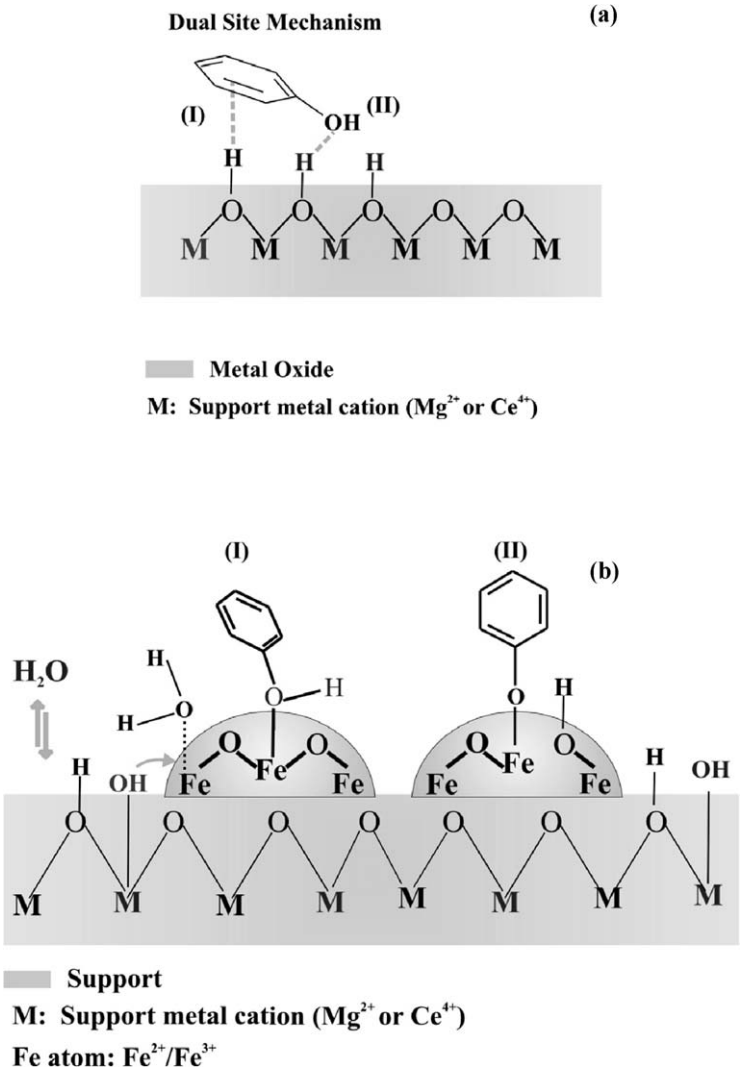

Scheme 1. (a) Adsorption mode mechanism of phenol during steam reforming reaction on MgO and CeO_2. (b) Adsorption mode of phenol and water over Mg-Ce-O supported iron oxides. The –OH back-spillover mechanism from the support to the iron oxide crystallites during phenol steam reforming is indicated.

3.5. Steam reforming of phenol in the presence of CO_2 absorbent

Fig. 10a presents transient response curves of H_2 production on the switch He → C_6H_5OH/H_2O/Ar/He at 650 °C over a catalytic bed (0.45 g) consisting of 5% Fe/Mg-Ce-O mixed with SiO_2 or dolomite DOLII (1:2 w/w), and also of DOLII mixed with SiO_2 (2:1 w/w). The figure also shows the theoretical transient response curve of H_2 that would be obtained if no AER effect were present (i.e., the sum of H_2 response curves due to Fe/Mg-Ce-O and DOLII alone). Based on this analysis, the Fe/Mg-Ce-O catalytic system had higher H_2 product concentrations (solid line) in the presence of DOLII than in the absence of DOLII during the first 20 min of reaction. After 20 min on reaction stream, the estimated AER was about 27%, compared with 80% at shorter reaction times (e.g., 5 min). In other words, an 80% increase in H_2 production was obtained when DOLII was present in the catalytic bed along with the Fe/Mg-Ce-O catalyst after 5 min of reaction. It should be noted here that the Ar response curve (not shown in Fig. 10) appeared very close to the y-axis; thus, the time delay of about 2.5 min observed in Fig. 10 is due purely to kinetic effects related to the steam reforming of phenol reaction.

As seen in Fig. 10a (solid line), the transient H_2 production was always larger than the theoretical H_2 production. It should be clarified at this point that after about 30 min of reaction, the experimental response of H_2 concentration due to the AER effect became similar to the theoretical one, as would be expected. This is true because CO_2 chemisorption on DOLII under phenol steam reforming reaches a saturation value, and thus the AER effect should become zero. The time of saturation of DOLII with CO_2 depends on various parameters, including the number of sites for CO_2 chemisorption per gram of solid (DOLII and Mg-Ce-O support), the actual CO_2 gas concentration around the solid particles, the reaction temperature, and the heat of CO_2 chemisorption related to DOLII and Mg-Ce-O solids. The results of Fig. 10a demonstrate that DOLII is a suitable material for significantly enhancing H_2 formation in phenol steam reforming for short reaction times.

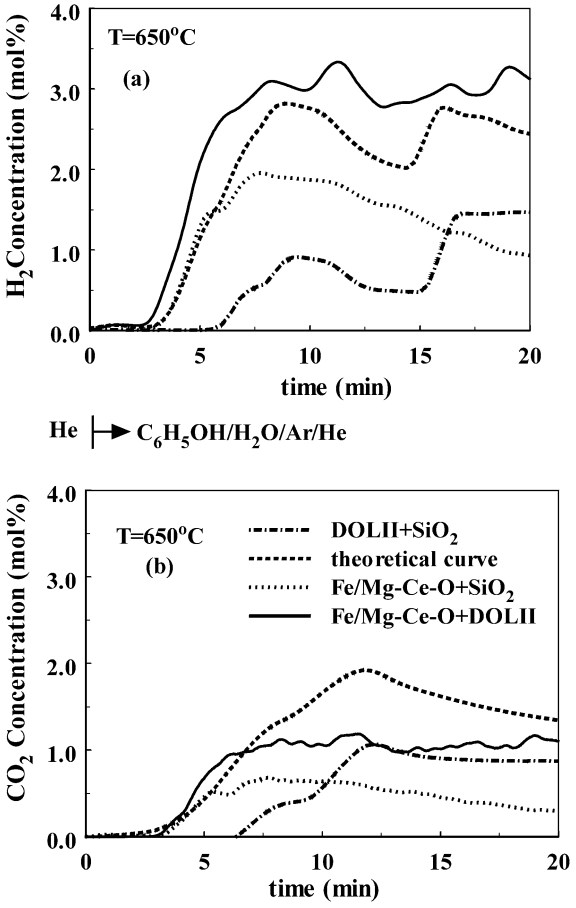

Fig. 10. Transient response curves of H_2 (a) and CO_2 (b) obtained at 650 °C over the 5 wt% Fe/50Mg-50Ce-O catalyst in the presence and absence of DOLII CO_2-absorbent, and over the DOLII alone according to the sequence: He → 0.25% C_6H_5OH/20% H_2O/Ar/He (t). The theoretical transient response curves of H_2 and CO_2 formation calculated as the sum of the corresponding curves due to Fe/Mg-Ce-O and DOLII alone are also presented. The weight ratio of Fe-based catalyst and DOLII in the catalytic bed is 1:2 (w/w). $W = 0.45$ g.

Fig. 10b shows transient response curves of CO_2 production corresponding to those of H_2. The CO_2 transient response during the first 20 min of reaction obtained over the Fe/Mg-Ce-O + DOLII catalytic bed appears to be lower than the theoretical one. Thus, DOLII is able to chemisorb additional CO_2 produced during phenol steam reforming. The CO_2 uptake by DOLII under phenol steam reforming cannot be estimated from the CO_2 transient response curves of Fig. 10b; therefore, the following experiment was designed to estimate the amount of CO_2 chemisorption under steam reforming of phenol reaction, confirming the AER process of phenol toward further H_2 production (Fig. 10a).

3.6. Probing the AER effect under steam reforming of phenol

After a 30-min phenol steam reforming reaction at 650 °C, in which practically no AER of phenol occurred (see Section 3.5), the feed was changed to pure He for 65 min until a low CO_2 signal was obtained (Fig. 11), at which point the temperature of the catalytic bed material was increased to 800 °C in He flow

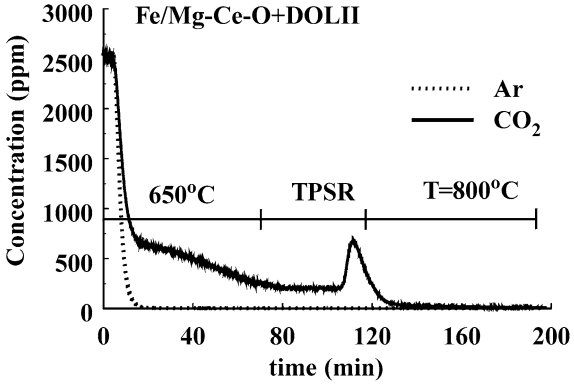

Fig. 11. Isothermal and TPSR response curves of Ar and CO_2 obtained in He flow following phenol steam reforming at 650 °C for 30 min over the 5 wt% Fe/50Mg-50Ce-O + DOLII catalytic bed material. The weight ratio of Fe/Mg-Ce-O and DOLII in the catalytic bed is 1:2 (w/w). $W = 0.45$ g.

(TPSR, $\beta = 25$ °C/min). Fig. 11 presents the transient response curves of Ar and CO_2 obtained under the isothermal and TPSR experimental runs over the Fe/Mg-Ce-O + DOLII catalytic bed. At $t = 0$, the CO_2 concentration was that obtained after a 5-min flush in He of the reactor effluent stream. The total amount of CO_2 uptake (determined by integrating the CO_2 response curve relative to the Ar curve) was found to be 327.5 μmol CO_2 per gram of catalytic bed. The amount of CO_2 desorbed is attributed to that absorbed by both DOLII and Mg-Ce-O solids during phenol steam reforming. To estimate the contribution of the Mg-Ce-O support to the total CO_2 uptake by the catalytic bed material, the same experiment was conducted over the Fe/Mg-Ce-O + SiO_2 catalytic bed. The estimated amount of CO_2 desorbed was 102 μmol CO_2/g. A blank experiment performed with SiO_2 alone showed no CO_2 uptake. Thus, the amount of CO_2 absorbed by DOLII after 30 min of phenol steam reforming was 225.5 μmol CO_2/g of catalytic bed material. This amount corresponds to only 20% of that estimated from CO_2 equilibrium chemisorption experiments (10 vol% CO_2/N_2) performed over DOLII at 650 °C using thermogravimetric analysis [26]. Due to the catalytic activity of DOLII, it is reasonable to expect some of the CO_2 chemisorption sites to be covered by carbonaceous deposits (active or inactive) which are found in the phenol steam reforming reaction path.

In the case of olivine (CO_2 absorbent material), the CO_2 uptake estimated under phenol steam reforming was found to be 33 μmol-CO_2/g of olivine. The natural CO_2 absorbent materials of olivine, A2 and A3, were no better in promoting the AER of phenol. CO_2 chemisorption experiments at 25 °C followed by TPD ($\beta = 30$ °C/min, $W = 0.3$ g) conducted over the DOLII and A3 solids revealed that a lower bonding strength of CO_2 on DOLII than on A3 ($T_M = 525$ °C vs. 720 °C). It appears that under phenol steam reforming reaction conditions, the amount of "carbon" deposits on the CO_2 absorbent material is an important parameter for determining the actual CO_2 uptake. Adsorption of water was found to weaken the bond between CO_2 and CaO [85] and to promote the sintering of MgO crystallites [86]. Furthermore, conversion of CaO to $Ca(OH)_2$ is possible under the given reaction conditions. These findings give reasonable explanations for the different AERs of phenol

promoted by CaO and MgO in the dolomites and calcite materials examined.

4. Conclusions

The following main conclusions can be derived from the results of the present work:

(a) The support chemical composition was found to strongly influence the rate of steam reforming of phenol toward H_2 formation, the CO/CO_2 product ratio, and the amount of "carbon" deposits over supported Fe catalysts in the 600–700 °C range.
(b) There was an optimum loading of Fe in the 1–10 wt% range (5 wt%) for maximum H_2 yields during steam reforming of phenol over Fe/50Mg-50Ce-O catalysts, whereas the amount of "carbon" deposits increased with increasing Fe loading.
(c) The stability of the 5 wt% Fe/Mg-Ce-O catalyst after consecutive *oxidation* → *reaction* (at 650 °C) and *oxidation* → *reduction* → *reaction* cycles of short duration was found to decrease only up to the sixth cycle for the former and up to the seventh cycle for the latter. However, only a 25% decrease in the initial rate was observed when an intermediate H_2 reduction step was applied, compared with a 60% decrease when no intermediate H_2 reduction step was applied. The initial reduction of Fe^{3+} to Fe^{2+}/Fe^0 is suggested to enhance H_2 product yield under short reaction times.
(d) DOLII CO_2 absorbent produced the greatest effect on improving the H_2 product yield under short reaction times in the steam reforming of phenol over the 5 wt% Fe/50Mg-50Ce-O catalyst, compared with olivine and calcite CO_2 absorbent materials.
(e) Mössbauer studies performed over various supported Fe catalysts revealed that Fe was present as Fe^{2+} and Fe^{3+} during phenol steam reforming, with the Fe^{2+}/Fe^{3+} ratio depending on the support chemical composition. In the most active 5 wt% Fe/Mg-Ce-O catalyst, 65% of the total iron was found in the Fe^{2+} oxidation state.
(f) The 5 wt% Fe/50Mg-50Ce-O catalyst developed in the present work performed very well in phenol steam reforming at 700 °C compared with a Ni-based commercial catalyst used in tar steam reforming. A significantly lower CO/CO_2 ratio was obtained with the former compared with that obtained with the latter. Thus, the Fe/Mg-Ce-O catalyst should be further investigated for practical use in the steam reforming of tar.

Acknowledgments

The authors acknowledge financial support from the European Union (5th FP) through the ENK-5-CT-2001-00545 research project, as well as from the Research Committee of the University of Cyprus.

References

[1] L. Devi, K.J. Ptasinski, F.J.J.G. Jansen, Biomass Bioenergy 24 (2003) 125, and references therein.
[2] D. Sutton, B. Kelleher, J.R.H. Ross, Fuel Process. Technol. 73 (2001) 155.
[3] L. Garcia, M.L. Salvador, J. Arauzo, R. Bilbao, Energy Fuels 13 (1999) 851.
[4] S. Rapagna, N. Jand, P.U. Foscolo, Int. J. Hydrogen Energy 23 (1998) 551.
[5] R. Coll, J. Salvadó, X. Farriol, D. Montané, Fuel Process. Technol. 74 (2001) 19.
[6] T.A. Milne, N. Abatzoglou, R.J. Evans, Biomass Gasifier Tars: Their Nature, Formation and Conversion, NREL/TP-570-25357, National Renewable Energy Laboratory, CO, USA, 1989.
[7] J. Imai, K. Tawara, Jpn. Kokai Tokkyo Koho 121 (1994) 13125, JP06031169 Chem. Abstr.
[8] J.N. Armor, Appl. Catal. A: Gen. 176 (1999) 159, and references therein.
[9] K. Murata, L. Wang, M. Saito, M. Inaba, I. Takahara, N. Mimura, Energy Fuels 18 (2004) 122.
[10] M.E.S. Hegarty, A.M. O'Conor, J.R.H. Ross, Catal. Today 42 (1998) 225.
[11] A. Orío, J. Corella, I. Narváez, in: Proceegings of Conference on Developments in Thermochemical Biomass Conversion, Banff, Canada, 1996, p. 1144.
[12] J. Delgado, M.-P. Aznar, J. Corella, Ind. Eng. Chem. Res. 36 (1997) 1535.
[13] V. Vassilatos, G. Taralas, K. Sjöström, E. Björnbom, Can. J. Chem. Eng. 70 (1992) 1008.
[14] P. Pérez, P.-M. Aznar, M.A. Caballero, J. Gill, J.A. Martin, J. Corella, Energy Fuels 11 (1997) 1194.
[15] J. Corella, J. Herguido, J. Gonzáles-Saiz, J. Trujillo, in: A.V. Bridgwater, J.L. Kuester (Eds.), Research in Thermochemical Biomass Conversion, Elsevier, London, 1988, p. 754.
[16] I. Narváez, A. Orío, M.P. Aznar, J. Corella, Ind. Eng. Chem. Res. 35 (1996) 2110.
[17] H. Aldén, E. Björkman, M. Carlsson, A. Waldheim, in: Proceedings of Conference on Advances in Thermochemical Biomass Conversion, Interlaken, Switzerland, 1992, p. 216.
[18] G. Lammers, A.A.C.M. Beenackers, in: Proceedings of Conference on Developments in Thermochemical Biomass Conversion, Banff, Canada, 1996, p. 1179.
[19] P.A. Simell, N. Hakala, H.E. Haario, Ind. Eng. Chem. Res. 36 (1997) 42.
[20] G. Taralas, V. Vassilatos, K. Sjöström, J. Delgado, Can. J. Chem. Eng. 69 (6) (1991) 1413.
[21] S. Rapagna, N. Jand, A. Kiennemann, P.U. Foscolo, Biomass Bioenergy 19 (3) (2000) 187.
[22] J. Corella, J.M. Toledo, R. Padilla, Energy Fuels 18 (2004) 713.
[23] J.R. Rostrup-Nielsen, Catal. Sci. Technol. 4 (1984) 1.
[24] A.R. Brun-Tsekhovoi, A.N. Zadorin, Y.R. Katsobashvili, S.S. Kourdyumov, in: Proceedings of the World Hydrogen Energy Conference, vol. 2, Pergamon, New York, 1986.
[25] B.T. Carvil, J.R. Hufton, S. Sircar, AIChE J. 42 (1996) 2765.
[26] European project, 5th FP, ENK5-CT-2001-00545. A New Approach for the Production of a Hydrogen-Rich Gas from Biomass-An Absorption Enhanced Reforming Process.
[27] M. Specht, A. Bandi, F. Baumgart, T. Moellenstedt, O. Textor, T. Weimer, in: Z.Q. Mao, T.N. Veziroglou (Eds.), Hydrogen Energy Progress XIII, 2000.
[28] K. Polychronopoulou, C.N. Costa, A.M. Efstathiou, Appl. Catal. A: Gen. 272 (2004) 37.
[29] K. Polychronopoulou, J.L.G. Fierro, A.M. Efstathiou, J. Catal. 228 (2004) 417.
[30] M.I. Zaki, H.M. Ismail, R.B. Fahim, Surf. Interf. Anal. 8 (1986) 185.
[31] A. Guiner, X-Ray Diffraction in Crystals, Imperfect Crystals and Amorphous Bodies, Dover Publications Inc., New York, 1994.
[32] D. Wang, S. Czernik, D. Montané, M. Mann, E. Chornet, Ind. Eng. Chem. Res. 36 (1997) 1507.
[33] H.C. Yao, Y.F. Yao, J. Catal. 86 (1984) 254.
[34] G.A.H. Mekhemmer, H.M. Ismael, Colloids Surf. Eng. Aspects 235 (2004) 129.

[35] (a) S. Damyanova, C.A. Perez, M. Schmal, J.M.C. Bueno, Appl. Catal. A: Gen. 234 (2002) 271;
(b) B.M. Reddy, A. Khan, Y. Yamada, T. Kobayashi, S. Loridant, J.-C. Volta, J. Phys. Chem. B 107 (2003) 11475.
[36] D. Szmigiel, W. Raró'g-Pilecka, E. Miśkiewicz, M. Gliński, M. Kielak, Z. Kaszkur, Z. Kowalczyk, Appl. Catal. A: Gen. 273 (2004) 105.
[37] A. Trovarelli, M. Boaro, E. Rocchini, C. de Leitenburg, G. Dolcetti, J. Alloys Compd. 323 (2001) 584.
[38] F. Giordano, A. Trovarelli, C. de Leitenburg, M. Giona, J. Catal. 193 (2000) 273.
[39] M.P. Rosynek, Catal. Rev.-Sci. Eng. 16 (1977) 111.
[40] A. Pineau, N. Kanari, I. Gaballah, Thermochim. Acta, in press.
[41] G. Munteanu, D. Iliaeva, D. Andeeva, Thermochim. Acta 291 (1997) 171.
[42] B. Gillot, J. Tyranowicz, A. Rousset, Mater. Res. Bull. 10 (1975) 775.
[43] E.E. Unmuth, L.H. Schwartz, J.B. Butt, J. Catal. 63 (1980) 404.
[44] N. Lingaiah, P.S. Sai Prasad, P. Kanta Rao, L.E. Smart, F.J. Berry, Appl. Catal. A: Gen. 213 (2001) 189.
[45] M. Boudart, A. Delbouille, J.A. Dumesic, S. Khammouma, H. Topsøe, J. Catal. 37 (1975) 486.
[46] J.A. Navío, M.C. Hidalgo, G. Colon, S.G. Botta, M.I. Litter, Langmuir 17 (2001) 202.
[47] M.D. Shroff, D.S. Kalakkad, K.E. Coulter, S.D. Köhler, M.S. Harrington, N.B. Jackson, A.G. Sault, A.K. Dayte, J. Catal. 156 (1995) 185.
[48] E. Perkin, Handbook of X-Ray Photoelectron Spectroscopy, Minn. Physical Electronics Publication, Eden Praire, 1992.
[49] X.Z. Jiang, A. Stevenson, J.A. Dumesic, J. Catal. 91 (1985) 11.
[50] C.R.F. Lund, J.A. Dumesic, J. Catal. 72 (1981) 21.
[51] J.-F. Lee, M.-D. Lee, P.-K. Tseng, Appl. Catal. 52 (1989) 193.
[52] P.P. Vaishnava, P.I. Ktorides, P.A. Montano, K.J. Mbadcam, G.A. Melson, J. Catal. 96 (1985) 301.
[53] J. Galuszka, T. Sano, J.A. Sawicki, J. Catal. 136 (1992) 96.
[54] B.J. Tatarchuk, J.A. Dumesic, J. Catal. 70 (1981) 323, and references therein.
[55] M. Alifanti, B. Baps, N. Blangenois, J. Naud, P. Grange, B. Delmon, Chem. Mater. 15 (2003) 395.
[56] J.A. Navío, M.C. Hidalgo, G. Colon, S.G. Botta, M.I. Litter, Langmuir 17 (2001) 202.
[57] F.J. Perez-Alonso, I. Melián-Cabrera, M. López Granados, F. Kapteijn, J.L.G. Fierro, J. Catal. 239 (2006) 340.
[58] J.W. Niemantsverdriet, A.M. van der Kraan, W.L. van Dijk, H.S. van der Baan, J. Phys. Chem. 84 (1980) 3365.
[59] J.W. Niemantsverdriet, H.S. van der Baan, W.N. Delgass, M.A. Vannice, J. Phys. Chem. 89 (1985) 67.
[60] A.M. van der Kraan, Hyperfine Interact. 40 (1988) 211.
[61] G.L. Caër, J.M. Dubois, J.P. Senateur, J. Solid State Chem. 19 (1976) 19.
[62] A. Pattek-Janczyk, B. Miczko, W.A. Morawski, Appl. Catal. A: Gen. 141 (1996) 1.
[63] R. Spretz, S.G. Marchetti, M.A. Ulla, E.A. Lombardo, J. Catal. 194 (2000) 167.
[64] M. Boudart, A. Delbouille, J.A. Dumesic, S. Khammouna, H. Topsøe, J. Catal. 37 (1975) 486.
[65] J.A. Dumesic, H. Topsøe, S. Khammouna, M. Boudart, J. Catal. 37 (1975) 503.
[66] M. Sanchez, J. Gazquez, J. Catal. 104 (1987) 120.
[67] A.R. West, Basic Solid State Chemistry, Wiley, New York, 1988.
[68] T.V. Reshetenko, L.B. Andeeva, V.A. Ushakov, E.M. Moroz, A.N. Shmakov, V.V. Kriventsov, D.I. Kochubey, Yu.T. Pavlyukhim, A.L. Chuvilin, Z.R. Ismagilov, Appl. Catal. A: Gen. 270 (2004) 87.
[69] K. Polychronopoulou, C.N. Costa, A.M. Efstathiou, Catal. Today 112 (2006) 89, and references therein.
[70] Y. Schuurman, C. Marquez-Alvarez, V.C.H. Kroll, C. Mirodatos, Catal. Today 46 (1998) 185.
[71] L. Garcia, R. French, S. Czernik, E. Chornet, Appl. Catal. A: Gen. 201 (2000) 225.
[72] M. Asadullah, S. Ito, K. Kunimori, M. Yamada, K. Tomishige, J. Catal. 208 (2002) 255.
[73] A. Piras, A. Trovarelli, G. Dolcetti, Appl. Catal. B: Environ. 28 (2000) L77.
[74] M.C.J. Bradford, M.A. Vannice, Catal. Today 50 (1999) 47.
[75] S. Wang, G.Q. Lu, Appl. Catal. B: Environ. 19 (1998) 267.
[76] S. Hilaire, X. Wang, T. Luo, R.J. Gorte, J. Wagner, Appl. Catal. A: Gen. 215 (2001) 271.
[77] J. Corella, J.M. Toledo, R. Padilla, Energy Fuels 18 (2004) 713.
[78] A. Orío, J. Corella, I. Narváez, Ind. Eng. Chem. Res. 36 (9) (1997) 3800.
[79] J. Corella, M.A. Caballero, M.-P. Aznar, C. Brage, Ind. Eng. Chem. Res. 42 (13) (2003) 3001.
[80] U.S. Yadar, B.D. Pandey, B.K. Das, D.N. Jena, Ironmaking Steelmaking 29 (2002) 91.
[81] T. Morimoto, Y. Suda, M. Nagao, J. Phys. Chem. 89 (1985) 4881.
[82] W. Pohle, J. Chem. Soc. Faraday Trans. 78 (1982) 2101.
[83] M. Nakazawa, G.A. Somorjai, Appl. Surf. Sci. 84 (1995) 309.
[84] M. Nakazawa, G.A. Somorjai, Appl. Surf. Sci. 68 (1993) 517.
[85] Y. Wang, W.J. Thomson, Chem. Eng. Sci. 50 (1995) 1373.
[86] D.T. Beruto, R. Vecchiattini, M. Giordani, Thermochim. Acta 404 (2003) 25.